Stony Brook University

Epitaxial Growth of Hexagonal Ferrite Films by Thermal Spray

A Thesis Presented

By

Mei-Ni Chou

to

The Graduate School

in Partial Fulfillment of the

Requirements

for the Degree of

Master of Science

in

Materials Science and Engineering

Stony Brook University

August 2007

Stony Brook University

The Graduate School

Mei-Ni Chou

We, the thesis committee for the above candidate for the
Master of Science degree, hereby recommend
acceptance of this thesis

Dr. Richard J. Gambino, Professor, Thesis Advisor
Department of Materials Science and Engineering

Dr. Michael Dudley, Professor
Department of Materials Science and Engineering

Dr. Andrew Gouldstone, Assistant Professor
Department of Materials Science and Engineering

This thesis is accepted by the Graduate School

Lawrence Martin
Dean of the Graduate School

Abstract of the Thesis

Epitaxial Growth of Hexagonal Ferrite Films by Thermal Spray

by

Mei-Ni Chou

Master of Science

In

Materials Science and Engineering

Stony Brook University

2007

Films of hexaferrite ($BaFe_{12}O_{19}$ and $SrFe_{12}O_{19}$, known as BaM and SrM) were grown onto hexagonal Al_2O_3, cubic MgO, and cubic gadolinium gallium garnet (GGG) substrates by flux growth. Different ratios of ferrite to flux (Bi_2O_3) were also studied using the same substrate, c-axis Al_2O_3. These films were examined for magnetic properties, structure, and surface morphology. Magnetic hysteresis results show that for a heat treatment temperature of 1000°C the BaM film had highest magnetic anisotropy on (110) MgO, apparently, due to formation of c-axis oriented BaM. A higher ratio of BaM and SrM in the flux/ferrite mixture produced higher magnetization hysteresis loops. SrM films were ferromagnetic and had large coercivity when the amount of ferrite was increased to 10 mol%. C-axis oriented hexagonal crystals are clearly seen in SEM images on both BaM and SrM films heated at 1000°C. Epitaxial films produced by flux growth can be used in thermal spraying and post-annealing to produce thicker coatings enhanced with magnetic properties, c-axis epitaxial growth, and hexaferrite M crystal structure.

Table of Contents

List of Figures

List of Tables

Acknowledgement

I would like to express my sincere gratitude and appreciation to Prof. Richard J. Gambino, my advisor, for his continuous advice, encouragement and support throughout the course of this study. I would also like to thank Shan Shan Liang for the help she gave in running some of the analytical experiments.

1. Introduction

Hexagonal ferrites, such as barium ferrite ($BaFe_{12}O_{19}$) and strontium ferrite ($SrFe_{12}O_{19}$), have received much interest in recent years for microwave device applications. Due to its high uniaxial anisotropy and large resistivity, barium ferrite is especially of interest for use in hybrid microwave devices, monolithic microwave integrated circuits or even as a future replacement for yttrium iron garnet [1].

The next generation of magnetic microwave devices (isolators, filters, phase shifters, and circulators and related components) will be planar, self-biased, and low loss, and operate better than today's devices [2]. High quality c-axis oriented thick (>300 μm) BaM films that can be self-biased to eliminate the requirement of an external magnetic field are needed for this application.

Epitaxial hexagonal ferrite films can be grown by many methods, such as sputtering, pulsed laser deposition (PLD), chemical vapor deposition (CVD), and liquid phase epitaxy (LPE), etc. In this study, we propose a new process for the growth of thick epitaxial BaM and SrM films by combination of flux growth and thermal spray technology. The growth experiments in this study are limited to methods for the growth of epitaxial seed layers for subsequent thermal spray deposition. Developing process conditions for thermal spray epitaxy is beyond the scope of this work.

2. Rationale

2.1. Magnetic Anisotropy

Directional preference of magnetization is called magnetic anisotropy. There are several different types of anisotropy, such as magnetocrystalline, shape, and stress. Magnetocrystalline anisotropy is very strong in hexagonal ferrites and is important for its microwave applications. Magnetocrystalline anisotropy can be most easily seen by measuring magnetization curves along different crystal directions. For example, barium ferrite easily saturates along the c-axis of hexagonal structure which is the easy direction of magnetization; the hard direction is in the basal plane.

2.2. Hexagonal Ferrite

Barium Ferrite ($BaFe_{12}O_{19}$) and strontium ferrite ($SrFe_{12}O_{19}$) are the most important hexagonal ferrites, and are used mostly as permanent magnets. They have the magnetoplumbite structure which has 32 atoms/formula unit and 64 atoms in a single unit cell (see Fig. 1). The structures are given the notations, BaM and SrM, respectively. Hexagonal ferrite has a strong anisotropy with the easy direction along the c axis (H_A~17000 Oe). The high magnetic anisotropy field can be adjusted by appropriate substitution for Fe and Ba or Sr ions allowing tuning of resonance frequencies from 1-100 GHz [3]. The saturation magnetization is small, $4\pi M\mathrm{s} \approx 4-5\mathrm{KG}$, therefore, their c-axis anisotropy is sufficient to overcome the magnetostatic energy, $2\pi M_S^2 \approx 8\times10^4\,\mathrm{J/m^3}$, and give perpendicular magnetization in either the flat hexagonal platelets or in (0001) textured films. Fig. 1 shows that the BaM structure consist of seven ferric ions distributed onto five interstitial sites (one trigonal bipyramidal, two octahedral, and two tetrahedral). Strontium ferrite is almost identical to $BaFe_{12}O_{19}$ in its crystallographic structure and magnetic properties, except that the sintered magnets generally have higher coercivity. The magnetic moments of the iron ions (Fe^{3+}) which lie along the c-axis are coupled to

each other by a superexchange interaction. The angle between the ferric cations and oxygen in Fe-O-Fe bonds determines their antiferromagnetism (i.e., larger exchange for larger angles). The ferromagnetic resonance (FMR) linewidth for a single crystal is reported to range from 10 to 20 Oe [2] [4].

Barium ferrite has a great advantage in microwave device applications due to its large uniaxial magnetic anisotropy, which essentially provides an internal biasing field that allows the material to produce resonances at frequencies larger than 50 GHz without large applied magnetic fields. The application of bulk BaM has been demonstrated, and it has been shown orientated polycrystalline BaM can be used in nonreciprocal devices, such as circulators, isolators, and phase shifters, whereas single BaM is used in tunable filters and oscillators [5].

3. Literature review on epitaxial films of hexagonal ferrite

Hexagonal ferrites, such as barium ferrite and strontium ferrite films [6-8] have been deposited by many methods. Dorsey, *et al.* [9] grew epitaxial thin films of barium ferrite on basal plane sapphire by pulsed laser deposition (PLD). They obtained a derivative ferromagnetic resonance (FMR) linewidth of 66 Oe at 58 GHz. However, the reported value of the linewidth for bulk single-crystal BaM is as low as 6-30 Oe [10]. Since then much research effort has been put into making an epitaxial BaM film with low FMR linewidths. Shinde, *et al.* [10-12] reported the effect of thin film deposition conditions, such as deposition temperature, oxygen pressure, etc., and substrate-induced lattice strains on the structure and magnetic properties of epitaxial BaM films grown by PLD. The best film reported by Song, *et al.* [13] had a thickness of 0.85 μm and a half power main mode FMR linewidth of 27 Oe at 60.3 GHz which is almost the same as for bulk crystals. Although PLD has been shown to produce high quality thin films, attempts to produce thicker films resulted in stressed or cracked films with extremely large linewidths [5, 14]. Song, *et al.* found thicker films separated from substrate during the annealing process [13]. The high crystal quality BaM films deposited by PLD had perpendicular magnetic anisotropy and low microwave losses; however, the thickness of the films is still too thin for practical microwave devices.

Therefore, many researchers have changed their deposition technique from PLD to liquid-phase epitaxy (LPE) technique in order to produce a thicker film with improved FMR linewidth, which has proven to be a more effective way to grow thick films so far [15, 16]. Usually, the deposition of seed layers of BaM onto the substrate by PLD or sputtering is required to form a thicker film when using LPE [15, 17]. Wang, *et al.* [17] have deposited BaM films on both sides of a magnesium oxide, (111) MgO, substrate by LPE. The total thickness of BaM film was about 45 μm and the ferromagnetic resonance linewidth at 60 GHz is 27 Oe. However, thicker films need longer time, and the growth condition should be improved in order to reduce the growth time for industrial use. Yoon, *et al.* [15] have reported double-sided BaM films on m-planes ([1$\underline{1}$00] or [10$\underline{1}$0]) sapphire (Al_2O_3) substrate by modified LPE which requires seed layers, using pulsed laser ablation

deposition prior to the LPE deposition. They obtained thick films which had total thickness ranging from 60 μm to 200 μm and FMR linewidth of 80 Oe at 59.9 Hz for 70 μm thick films. The 2 hours deposition time is relatively shorter than the growth time of BaM films on (111) magnesium oxide (6-8 hours) by PLE technique. They also showed no evidence of delamination up to thickness of 70 μm whereas films grown by PLD started to delaminate for a thickness of >20 μm .

Kranov, *et al.* [16] demonstrated a modified liquid phase epitaxy (MLPE) method for growing of c-axis oriented polycrystalline BaM films which can be self-biased. They grew BaM films with thickness of up to 0.5 mm without a BaM seed layer, which greatly simplifies the fabrication process. The coercivity of the 350 μm thick film is about 100 Oe for the perpendicular orientation. They believe that a slower cooling rate during the process of crystallization could improve the coercivity. However, they still need to determine the FMR linewidth of the films.

LPE technique is more desirable to produce high-quality, thick BaM films compared to PLD technique but still not ideal. The quality of thick films by LPE still needs to be improved in order to be ideal for application in microwave devices. Moreover, LPE has difficulties and cost associated with upgrading this technique to production units capable of high throughput [2].

4. Lattice mismatch

Large growth stress could occur in BaM films during film growing process and then cause film cracking or delamination. The induced stress may be due to two effects as (1) Lattice constant mismatch, ε, between the BaM film and substrate. (2) Thermal expansion coefficient mismatch between the BaM film and substrate. Shinde, *et al.* [10] have studied the effects of these strains on the structure and magnetic properties of BaM thin film grown on sapphire. They found that reducing the mismatch-induced strain greatly decreases the FMR linewidth of the film. Therefore, it is essential to choose a suitable substrate material for growing high quality epitaxial BaM films [14, 15]. Table 1 and Table 2 show the mismatch of lattice constant and thermal expansion coefficient, respectively, between BaM, SrM and various substrate materials, sapphire (Al_2O_3), magnesium oxide (MgO), gadolinium gallium garnet (GGG), and $SrTiO_3$, which all are mostly used for epitaxial growth. Table 3 shows the melting point of the substrate materials which all have higher melting temperature than the ferrites (i.e. the melting point of barium ferrite is 1565°C).

Single-crystal sapphire (Al_2O_3) substrates were used to obtain good quality BaM films in most of the reports on BaM [5, 9-13, 15, 16, 18, 19]. Sapphire has the same structure as BaM, hexagonal structure but the lattice constant mismatch is quite large. The room temperature lattice mismatch has been estimated at 7% by comparing the areas of the sapphire and BaM oxygen planes [20], however, it has been shown that BaM can grow epitaxially on basal plane Al_2O_3. Fig. 2(a) shows the atomic structure of the surface (0001) planes in Al_2O_3 and BaM unit cells (with sapphire being smaller), where it has been noted that a shear strain is also present at the interface due to the lattice mismatch [12]. Fig. 2 (b) and (c) show surface (100) MgO and (11O) plane view compared with (0001) SrM plane, respectively. The mismatch between [110]MgO and $\frac{1}{3}[11\bar{2}0]_{SrM}$ is 3.44% (Table 1).

Table 2 shows that sapphire and MgO are not good lattice matches for barium ferrite (comparing the a-axis expansion). $SrTiO_3$ and GGG looks like a better match than sapphire and MgO. We chose some substrates form them to grow BaM films and the

coefficient of thermal expansion and lattice mismatch effects on the epitaxial growth of hexaferrite films was studied.

	a (Å)	c (Å)	Mismatch between $\langle 100\rangle_{sub}$ / $\frac{1}{3}\langle 11\bar{2}0\rangle_{BaM}$	$\langle 110\rangle_{sub}$	Mismatch between $\langle 110\rangle_{sub}$ / $\frac{1}{3}\langle 11\bar{2}0\rangle_{BaM}$
			$\frac{a_{substrate}-a_{BaM}}{a_{substrate}}$	$\sqrt{2}a_{substrate}$	$\frac{\sqrt{2}a_{substrate}-a_{ferrite}}{\sqrt{2}a_{substrate}}$
Al_2O_3 (Hexagonal)	4.785[21]	12.991[21]	-23.09%	--	--
MgO (cubic)	4.313[21]	--	-36.56%	6.10	+3.44%
SrTiO3 (cubic)	3.905[22]	--	--	5.52	-6.7%
GGG (cubic)	12.383	--	--	6.19($\frac{1}{2}a$)	+4.85%
BaM (Hexagonal)	5.89[10]	23.192	--	--	--
SrM (Hexagonal)	5.87[4]	23.1	--	--	--

Table 1 Mismatch of lattice constant between BaM and various substrate materials (Notation "–"means BaM under compressive stress; "+" means BaM under tensile stress.)

	Coefficient of Thermal Expansion (°C $^{-1}$)
Al_2O_3 (Hexagonal)	α_a 8.75×10^{-6}, α_c 7.88×10^{-6} (0~1027°C)[21]
Al_2O_3 (Rhombohedra)	7.8×10^{-6}
MgO	13.63×10^{-6} (25~1000°C)[21]
SrTiO3	10.4×10^{-6}
GGG	9.18×10^{-6}
BaM	α_a 10×10^{-6}, α_c 13×10^{-6} [23]
SrM	10×10^{-6}

Table 2 Substrate materials with a small thermal expansion mismatch (α_a is the CTE along a-axis and α_c is the CTE along c-axis).

	Al_2O_3	MgO	GGG	$SrTiO_3$
Melting Point	2040°C	2800°C	2098°C	2353°C

Table 3 Melting point of substrate materials

5. Experimental Procedures

5.1. Flux growth

Flux growth is a method commonly used for single crystal growth; it is also known as high temperature solution (HTS) growth. The flux is used as a solvent to dissolve the desired materials and decrease the melting point. The addition of flux results in the formation of low-melting-point eutectic, therefore, flux growth can be used, when the melting point is very high or too high for the facilities available to the operator. The main advantages of this method are that the crystals are grown below the melting temperature and the thermal strain is also minimized due to the relative low growth temperature [24]. Also reactions of the melt with crucibles and substrate materials are generally slower at lower temperature. Decomposition reactions can be avoided such as oxygen loss from ferrite melts.

Flux growth for single crystal films on substrates is usually used in liquid phase epitaxy technique (LPE). The $BaFe_{12}O_{19}$ flux melt for LPE growth has typically been prepared from a mixture of iron oxide (Fe_2O_3), barium carbonate ($BaCO_3$), and boron oxide (B_2O_3) [15-17] [25], however, the melting point is still too high, around 1200°C to 1300°C [17]. Yoo *et al.* [26] investigated the Bi_2O_3-BaO-B_2O_3 flux system mixed with barium ferrite (BaO + 6 Fe_2O_3). With this mixture it has been possible to decrease the growth temperature below 1000°C.

In the present study, barium ferrite powder was mixed with B_2O_3 and Bi_2O_3 by grinding in a mortar and pestle. The composition of the BaM mixed powder is $0.54BaO \cdot 0.36Fe_2O_3 \cdot 0.1B_2O_3$. Different mole ratios of Bi_2O_3 were added to the BaM powder. In order to let BaM interact with the flux better, the mixed powder was pressed into a pellet and sintered in a tube furnace at 700℃ for 5 hours. The pellet was then ground again in a mortar and pestle. Isopropyl alcohol was added to the sintered BaM mixture powder to make a paste and the paste was spread on the substrates. The samples were heated in a tube furnace at different temperatures (800-1000°C) for one hour in air. The heating rate and cooling rate were set at 10°C/min and 1°C/min, respectively. The

magnetic properties of the BaM samples were measured after heating using a Vibrating Sample Magnetometer (VSM) to determine the coercivity and the anisotropy of the coating. The surface images of the BaM films were examined on an optical microscopy and scanning electronic microscopy (SEM) to observe the shape and orientation of the crystals deposited on the substrate.

Different ratios of strontium ferrite ($SrFe_{12}O_{19}$), strontium carbonate ($SrCO_3$) and bismuth oxide (Bi_2O_3) were mixed together by grinding in a mortar and pestle. The mixed powders were then pressed into pellets and followed the same procedure as for BaM. The composition of the mixed powders is shown below:

1. 2.7mol% $SrFe_{12}O_{19}$ + 97.3mol% Bi_2O_3
2. 2.38mol%$SrFe_{12}O_{19}$ + 85.7mol% Bi_2O_3 +11.9 mol% $SrCO_3$
3. 4.16mol%$SrFe_{12}O_{19}$ + 75mol% Bi_2O_3 +20.84 mol% $SrCO_3$
4. 10mol%$SrFe_{12}O_{19}$ + 80mol% Bi_2O_3 +10 mol% $SrCO_3$
5. 20mol%$SrFe_{12}O_{19}$ + 70mol% Bi_2O_3 +10 mol% $SrCO_3$
6. 30mol%$SrFe_{12}O_{19}$ + 60mol% Bi_2O_3 +10 mol% $SrCO_3$

5.2. Thermal Spray

Thermal spray is an attractive and economical means of producing high performance coatings for the purpose of protecting materials and structures from a wide range of adverse environmental conditions. In thermal spray processing, feedstock material is melted and accelerated to high velocities, through either a combustion flame or a DC or RF thermal plasma arc. The droplets impinge on a substrate and rapidly solidify to form a thin “splat” (a flattened particle). The deposit is built up by successive impingement and interbonding of layered splats. The resulting microstructure and, thus, properties, vary depending on the processing conditions, spray parameters, materials and, in some cases, the substrate.

It has been shown how the temperature of the substrate effects the shape of the splats in thermal spray [27]. When the substrate temperature is above a specific point, defined as the transition temperature, the splats are mostly in disk-like shape and the

physical contact between the splat and the surface is improved. When the material particles are melted and spraying on the hot substrate, it is possible that substrate could easily melt also. If the substrate is preheated between the temperature of the sprayed particles and the transition temperature, the temperature gradient between the film and substrate, as shown in Fig. 3, could prevent the substrate melting at high temperature. We have selected high melting point substrates and added a flux to the seed layer to make it easy to get meltback when a molten droplet land on the growing ferrite coating. In our research, a substrate heater for epitaxially thermal spray was built and tested. The heater set up as shown in Fig. 6, and the temperature was read by a thermocouple attached on the surface of the heater. Fig. 7 shows the temperature on the heater surface by varying the voltage from 0 to 120 volts. The substrate heater can reach 780°C at 120 V.

The steps of epitaxial BaM film growth by thermal spray are explained below (Fig. 4);

First Growth

Preheated substrate for initial growth and epitaxial growth on single crystal substrate.

Later Growth

Cool substrate on the back surface with high heat flux from the plasma torch on the front surface and get melt back during growth.

For later growth, when the first growth film is located on a cool substrate (let the film below transition temperature), the first growth film will melt as ferrite particles are sprayed on the film. The film melts back and interacts with the sprayed particles to keep growing during the spraying. A temperature gradient diagram of the BaM film on cool substrate is shown in Fig. 5.

First Growth films and later growth films will be examined by VSM (perpendicular and parallel loops), XRD (for preferred orientation), and SEM (surface and cross section image).

5.3. Annealing

It has been shown that annealing procedures can refine the crystal structure and remove defects which would affect magnetic properties. For the hexagonal ferrite films grown by Ramamurthy, *et al.* [6], postannealing led to an increase in the magnetization, indicating incomplete formation of ferrite in the as-deposited state. Shinde, *et al.* [12] also showed that FMR linewidth could be further reduced and surface roughness can be improved after thermal annealing. It should be noted that there could be considerable diffusion of Al from sapphire substrate into BaM film at high annealing temperature. Diffusion of Al into BaM is known to decrease the magnetization, while enhancing the anisotropy and coercive field.

6. Characterization Measurements

6.1. Vibrating Sample Magnetometer (VSM)

The magnetic hysteresis loops (magnetization M vs. applied field H curves) for these films were measured using a VSM with a maximum field of 9000 Oe. Data were taken in both the parallel (H // film plane) and the perpendicular (H ⊥ film plane) geometries. The VSM system was calibrated with a Ni standard sample which has a mass of 36.9 mg and a saturation magnetization of 2.174 emu. The mechanism of the VSM is to measure the induced magnetization of the samples by mechanically vibrating them in a uniform magnetic field. The magnetic moment of the sample is measured by generating a signal voltage in pick up coils due to the time varying flux emanating from the vibrating sample. The output measurement displays the magnetic moment M as a function of the field H. Fig. 8 shows a schematic diagram of the VSM.

6.1.1. Barium Ferrite Films by Flux Growth

Barium ferrite films were prepared at different temperatures using the same substrate ((0001) Al_2O_3) and flux mixture (34 mol% BaM ($0.54BaO \cdot 0.36Fe_2O_3 \cdot 0.1B_2O_3$) + 66 mol % Bi_2O_3). The magnetic properties are shown in Fig. 9 to Fig. 11. The anisotropy of magnetization on BaM samples increases with heating temperature. Fig. 9 is the hysteresis loop of BaM prepared at 800°C. It shows that its parallel and perpendicular loops look the same, which means there is no anisotropy in the coating. It had small coercivity (Hc = 28 Oe for in-pane orientation, Hc = 12 Oe for out-of-plane), high field susceptibility from paramagnetic phase, and very small magnetization. At T = 900°C, Fig. 10 shows there is some anisotropy and the film still had low coercivity. Some nonmagnetic crystals (probably iron oxide or barium borate [17]) might form and were predominant in the growth of the film on the substrate. At 1000°C, as shown in Fig. 11, the film had large anisotropy and large coercivity (Hc = 1528 Oe for in-plane orientation, Hc = 1258 Oe for out-of-plane orientation). These properties indicate formation of BaM

phase and c-axis orientation (perpendicular) growth. A higher mole ratio of BaM (42.6 mol% BaM) was prepared at 1000°C on the same substrate. The film (Fig. 12) had clear hysteresis loops and smaller coercivity (Hc = 410 Oe for in-plane orientation, Hc = 344 Oe for out-of-plane orientation).

Fig. 13-16 are hysteresis loops for BaM (34 mol% BaM) films on different substrates, unspecified sapphire, (100) MgO, (110) MgO, and (111) GGG, heated at 1000°C for 1 hour. On unspecified sapphire, the hysteresis loop in Fig. 13 shows high coercivity and anisotropy. It had much larger magnetization and about twice as much as on c-axis sapphire (Table 5 shows the magnetization values of BaM coating on different substrates). On (100) and (110) MgO, the coating had very large magnetization and clearly some anisotropy, as shown in Fig. 14 and Fig. 15. The magnetization on (100) MgO is about 100 times lager than the sample on unspecified sapphire. They had very small coercivity (about 10 Oe). Table 6 shows the coercivity of BaM coatings on different substrates. The coating on MgO may have some formation of cubic ferrite ($MgFe_2O_4$). The easy axis of magnetization of BaM film is along the surface plane on MgO. This indicates that BaM probably grew along the in-plane direction (c-axis of BaM was aligned along the plane of MgO). Fig. 16 shows the properties of the film grown on GGG. There is a large paramagnetic signal from the GGG substrate. There was no BaM formed on GGG and the GGG was reacted with iron from BaM.

Table 6 lists the magnetization of BaM films on different substrates measured in fields of 9000 Oe and 2000 Oe. Magnetic anisotropy can be measured by the difference of the ratio of the parallel and perpendicular loops during the field between 2000 Oe to 9000 Oe. Anisotropy was calculated as, **Anisotropy = $S_{//}$ / $S_{\perp}$**. Anisotropy of 1.0 means isotropic. Table 6 indicates the BaM films on (100) MgO has the largest anisotropy.

6.1.2. Strontium Ferrite Films by Flux Growth

The mixed powder was prepared from the $SrCO_3$-Bi_2O_3 solvent by adding $SrFe_{12}O_{19}$ to form a series of compositions in which the mole ratio of ferrite to the solvent was varied. The magnetic properties of the SrM films were measured by VSM for each flux/ferrite composition. Fig. 17 displays that sample 1 had paramagnetic property and

some anisotropy. Sample 2 and 3 (Fig. 18 and Fig. 19) shows paramagnetic as well as small coercivity, but no anisotropy. For higher ratios of strontium ferrite, Sample 4, 5, and 6 had large coercivity ferromagnetic loops, as shown in Fig. 20-22. From the hysteresis loops of sample 4 to sample 6, the magnetization and coercivity increases as the mole ratio of strontium ferrite increase (Table 7 and 8).

6.2. Scanning Electronic Microscopy (SEM)

The surface images of the BaM and SrM films were analyzed under a SFEG-SEM from LEO 1550. Its electron gun is of a field emission type. An accelerating voltage of 20 kV was used. Back-scattered electron images were used to observe the different crystal phases. Chemical analysis in the SEM is performed by measuring the energy and intensity distribution of the X-ray signal generated by a focused electron beam. The X-ray spectrum is obtained by Energy-Dispersive analysis of X-ray (EDAX).

Fig. 23 to Fig. 25 are the SEM images of BaM films on c-axis Al_2O_3 at 800°C to 1000°C and the corresponding EDAX spectrums. On BaM film at 800°C, Fig. 23 shows two different kinds of square crystals, (b) and (c), which have crystals size ~ 50 μm. EDAX spectrums indicate that crystal (b) is a compound of Bi, Ba, and Fe; crystal (c) is a compound of Bi, Ba. On BaM film at 900°C, there are dark hexagons and light-colored square crystals, as shown in Fig. 24(a). Fig. 24(b) and (c) displays that the square crystal is a compound of Bi, Ba, and Fe; hexagonal crystals have more Ba, O, and Al. We suspect that the hexagons are barium ferrite which has some Al from the sapphire substrate. According to these surface images, the ferrite crystals might be covered with the flux containing Ba and Bi. Fig 25 (a) shows one hexagonal crystal on BaM film at 1000°C which has crystal size of 80 μm. Spiral growth patterns are clearly seen on barium ferrite hexagons. EDAX spectrum (Fig.25 (b)) also indicates that some Al interacted with BaM coating. 42 mol% BaM film also has barium ferrite hexagons (~85 μm) and bismuth iron oxide (square crystals), as shown in Fig. 26.

$SrFe_{12}O_{19}$ films which have different ratios of ferrite on c-axis Al_2O_3 and are prepared at 1000°C were also examined by SEM for surface images and chemical

analysis. Fig. 27(a) shows the image of the 4.16 mol% SrM film which has large square crystals (~200 μm) and small hexagonal crystals (ranging from10 to 60 μm). In Fig. 28(a), smaller dark particles (irregular shape and some hexagonal crystals) which have crystal size of 5 μm and large square crystals can be seen on the 10 mol% SrM film. Similar morphology can be found on 20 mol% and 30 mol% SrM films (Fig. 29(a) and Fig. 30 (a)) EDAX results shows that SrM films with higher ratio of $SrFe_{12}O_{19}$ have lesser Al effects on ferrite hexagons.

6.3. X-ray Diffraction (XRD)

X-ray diffraction was used to examine crystal structure in hexagonal ferrite films. The experiments were carried out with a Scintag/pad-v diffractometer with Cu Kα radiation (1.542 Å) and the tube operating at 45kV and 25mA.

Fig. 31 shows XRD spectrum on 34 mol% BaM film on c-axis sapphire substrate heated at 1000°C for 1 hour. The BaM film appeared to be some hexagonal $BaFe_{12}O_{19}$ and barium iron oxide compounds ($BaFe_2O_4$, $BaFeO_{2.84}$, and $Ba_5Fe_{14}O_{26}$). Fig. 32 shows XRD spectrum on 34 mol% BaM film on (110) MgO substrate heated at 1000°C for 1 hour. There was much more $BaFe_{12}O_{19}$ on MgO compared with the BaM film on c-axis sapphire. There might be small c-axis oriented 'nuclei' in these as-grown films, which can grow during the subsequent thermal spraying treatment.

Fig. 33 shows the XRD spectrum on 10 mol% SrM film on c-axis sapphire substrate heated at 1000°C for 1 hour. There were some hexagonal $SrFe_{12}O_{19}$, rhombohedral $BiFeO_3$, and monoclinic ε-Fe_2O_3 on SrM film.

7. Discussion And Conclusion

Hexagonal barium ferrite and strontium ferrite have been grown on different substrates (sapphire, MgO, and GGG), by heating in a tube furnace at various temperatures. Different mole ratios of the ferrite to the flux (bismuth oxide, Bi_2O_3) also have been studied using the same substrate, c-axis sapphire. These films have been examined for magnetic properties, structure, and surface morphology. The magnetic hysteresis results show that at different heat treatment temperatures the BaM films had different magnetic properties. The BaM films had ferromagnetic loops and magnetic anisotropy only for a heat treatment temperature of 1000°C. Presumably, c-axis oriented BaM formed when the heating temperature was higher than 1000°C and resulted in magnetocrystalline anisotropy. For the heating temperature of 1000°C, we found that the BaM films had the highest magnetic anisotropy on (110) MgO. According to the lattice mismatch between substrates and hexagonal ferrites (Table 1), MgO has the smallest mismatch. Fig. 34 indicates that lattice mismatch had a great effect on epitaxial growth of BaM films and the substrate which has smaller lattice mismatch can be used to produce a better epitaxial BaM film (higher anisotropy). Moreover, the BaM films on MgO substrates had an easy axis of magnetization along the substrate plane (parallel loops in Fig. 14 and Fig. 15). It indicates that BaM probably grew along the in-plane direction (c-axis of BaM was aligned along the (100) and (110) planes of MgO). From Table 2, MgO ($\alpha = 13.6\times10^{-6}$ °C^{-1}) has a good thermal expansion match compared with the coefficient of thermal expansion along the c-axis of BaM ($\alpha_c = 13\times10^{-6}$ °C^{-1}), which led the BaM preferably to grow along the <110> direction on MgO substrates. It is proved that the coefficient of thermal expansion and the lattice constant mismatch greatly affect the growth of well-orientated films.

A higher ratio of BaM and SrM in the flux/ferrite mixture produces higher magnetization hysteresis loops. SrM films were ferromagnetic and had large coercivity when the amount of ferrite was increased to 10 mol% or higher. The large coercivity from SrM films indicates that there might be single domain size in SrM crystals in the coating. These crystals formed in random orientation and resulted in no significant

anisotropy in all the SrM films. The VSM hysteresis loops (Fig. 20, Fig. 21, and Fig.22) show that there was not much difference in anisotropy between 10%, 20%, and 30% SrM films (The calculation for anisotropy is shown in Table 9 and plotted in Fig. 35). The magnetization increases with the amount of $SrFe_{12}O_{19}$, as shown in Fig. 36. The smallest magnetization occurs at about 8 mol% SrM (According to the linear fit line to the parallel magnetization parallel values in Fig. 36). This can be reasonably explained by using a hypothetical eutectic phase diagram of $SrFe_{12}O_{19}$ and $BaBiO_x$ (flux) with a eutectic composition of 8 mole% $SrFe_{12}O_{19}$. With 8 mol% SrM, the film has the least amount of $SrFe_{12}O_{19}$ phase and has smallest magnetization. The further the composition is from the eutectic the higher mole percentage of SrM formed, so the films have higher magnetization which comes from higher ratio of $SrFe_{12}O_{19}$ phase.

SEM images show some hexagonal crystals on both BaM and SrM films heated at 1000℃. Those hexagons were c-axis oriented and had spiral growth which originated from screw dislocations. Spiral growth patterns are clearly seen on barium ferrite hexagons in Fig 25. In Shinde, *et al.*'s work [12], it was shown that the growth of BaM on sapphire requires a significant distortion of BaM lattice. Screw dislocations are formed from shear strain between BaM and sapphire, and extend from the interface all the way to the film surface. The film growth occurs by adding atoms to a spirally winding step, which is known as "screw dislocation mediated island growth." In our study, the EDAX spectrums also indicate that some Al interacted with barium ferrite and strontium ferrite crystals. There were also some square crystals from barium iron oxide or bismuth iron oxide compounds (from flux) which could affect the magnetic properties of the hexaferrite films. The surface images didn't show a great amount of ferrite crystals which might be covered with the flux containing Ba and Bi. Further deposition by thermal spraying barium ferrite on flux growth films can be used to melt the flux films and increase the amount of ferrite crystals.

XRD results did not show evidence of epitaxial barium ferrite films with c-axis orientation. However, some barium ferrite and strontium ferrite (random orientation) can be seen in the XRD patterns, as well as some other compounds (i.e., barium iron oxides or bismuth iron oxides).

Epitaxial films produced by flux growth can be used in thermal spray and post-annealing to produce thicker coatings with enhanced magnetic properties, c-axis epitaxial growth, and hexaferrite M crystal structure. Since thicker films (>300 μm) are required in recent years for magnetic microwave devices, thermal spray technology will be an economic and efficient way to grow thick hexagonal ferrite films.

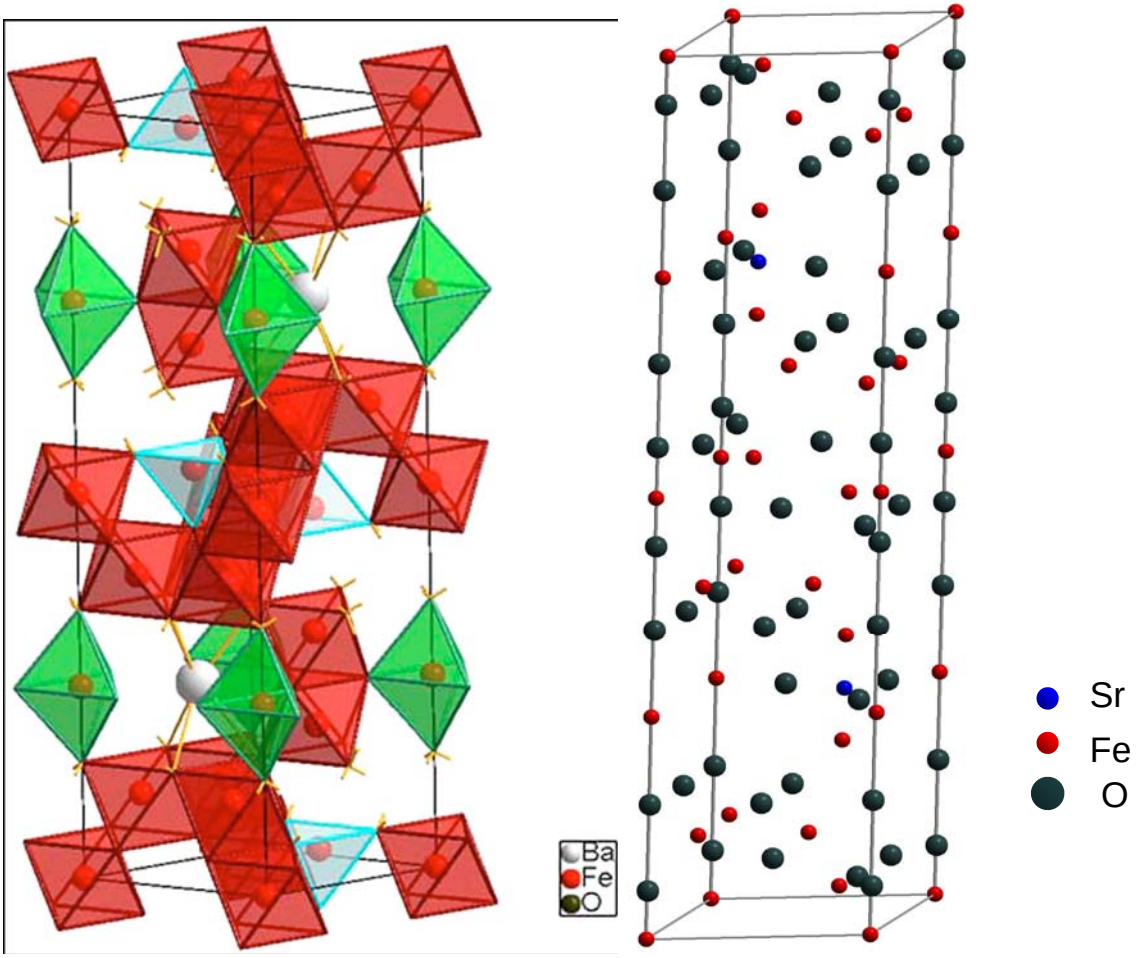

(a) (b)

Figure 1 (a) Color online Schematic diagram of the Ba-hexaferrite M-type structure. Ferric cations are depicted as residing in five sites depicted as tetrahedral, octahedral, and trigonal bipyramidal. From V. G. Harris, J. Appl. Phy. 99, 08M911, 2006 [2] **(b)** Schematic diagram of strontium ferrite unit cell structure.

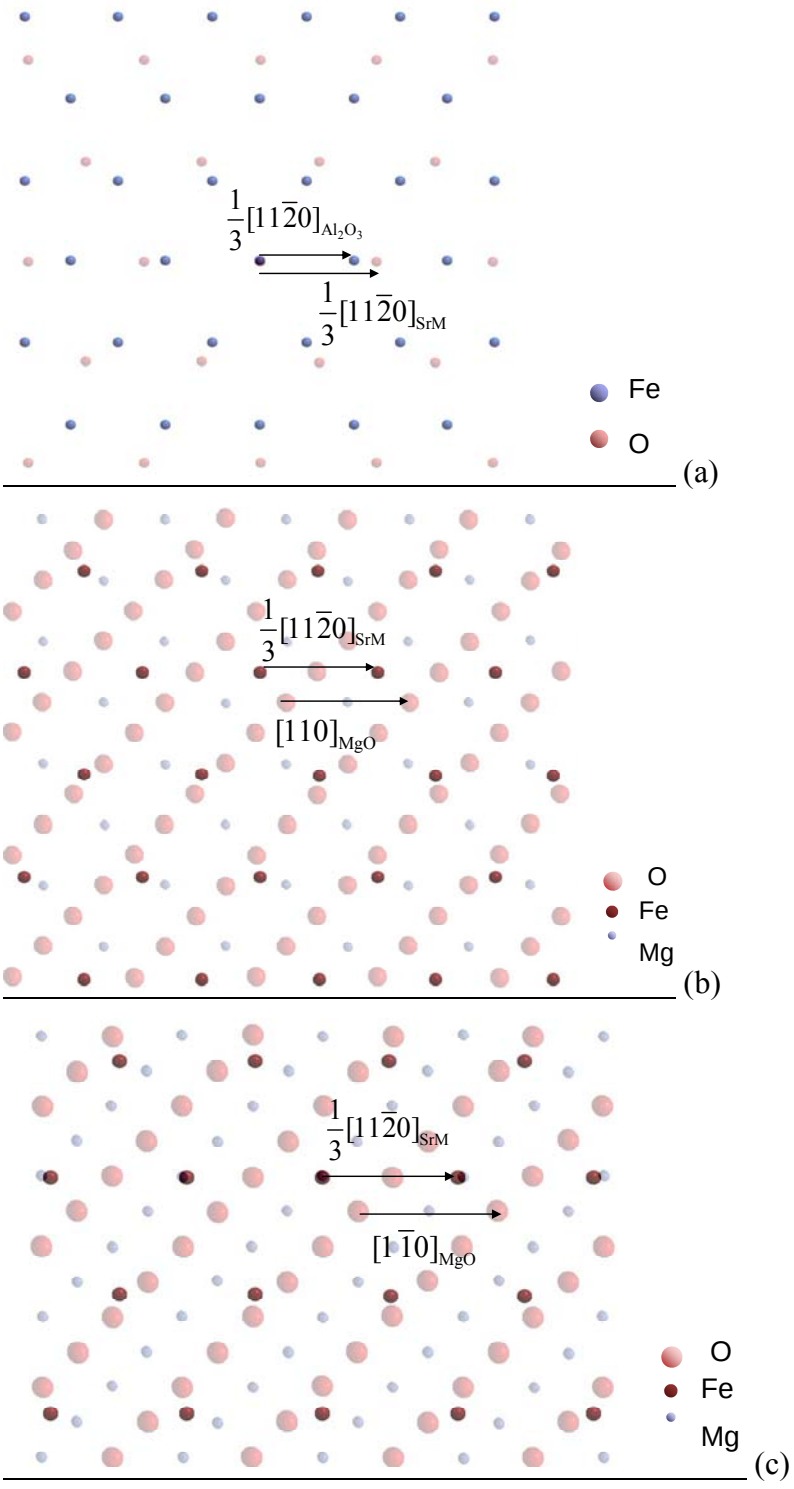

Figure 2 (a) Surface (0001) plane view of SrM (iron area) and hexagonal sapphire (oxygen area). The lattice mismatch is 23.09%. **(b)** Surface (100) MgO plane view compared with (0001) SrM plane. The mismatch between $[110]_{MgO}$ and $\frac{1}{3}[11\bar{2}0]_{SrM}$ is 3.44%. **(c)** Surface (110) MgO plane view compared with (0001) SrM plane.

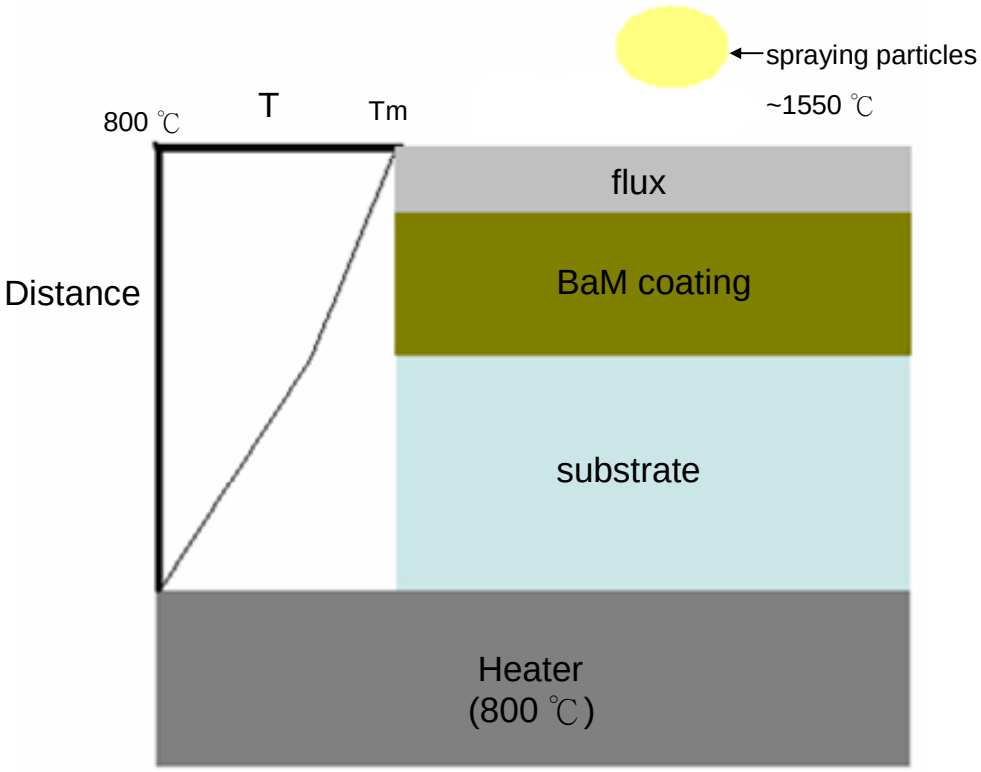

Figure 3 Temp Gradient diagram.

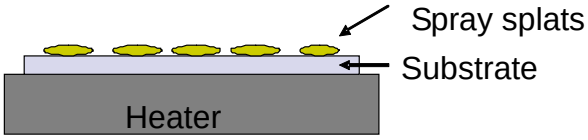

(a)

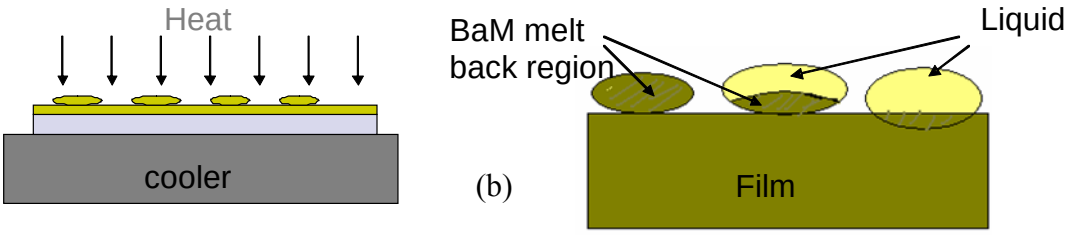

(b)

Figure 4 (a) Preheated substrate for initial growth and expitaxial growth will be on single crystal substrate.

(b) Cool substrate with high heat flux from the plasma torch and get meltback during growth.

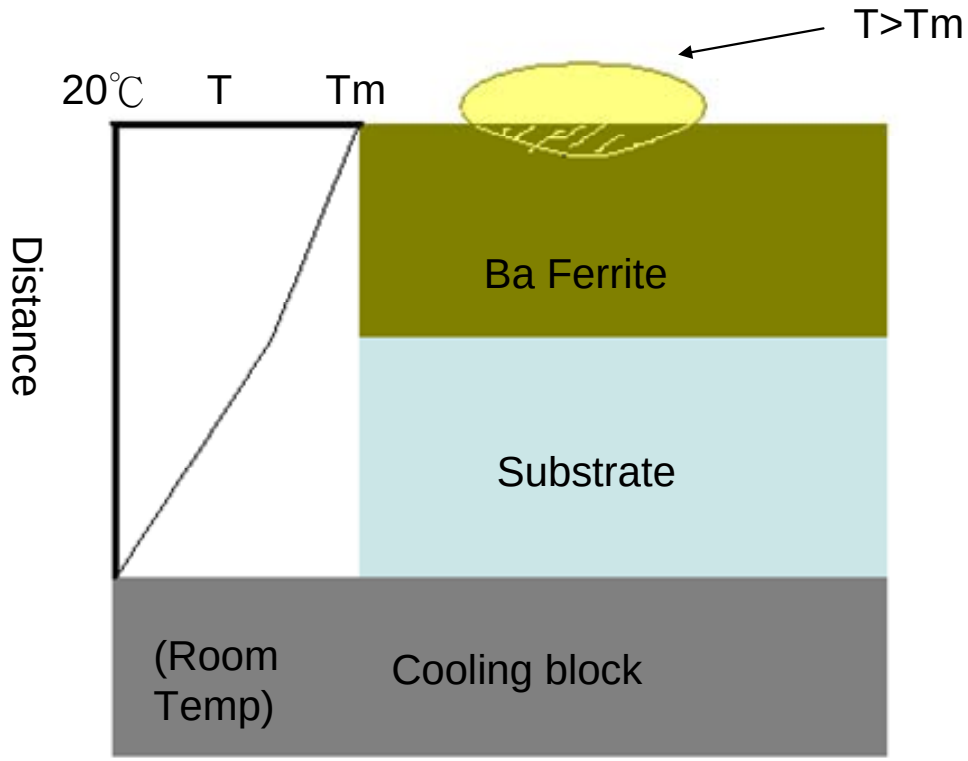

Figure 5 Temp Gradient diagram (meltback splat on BaM film).

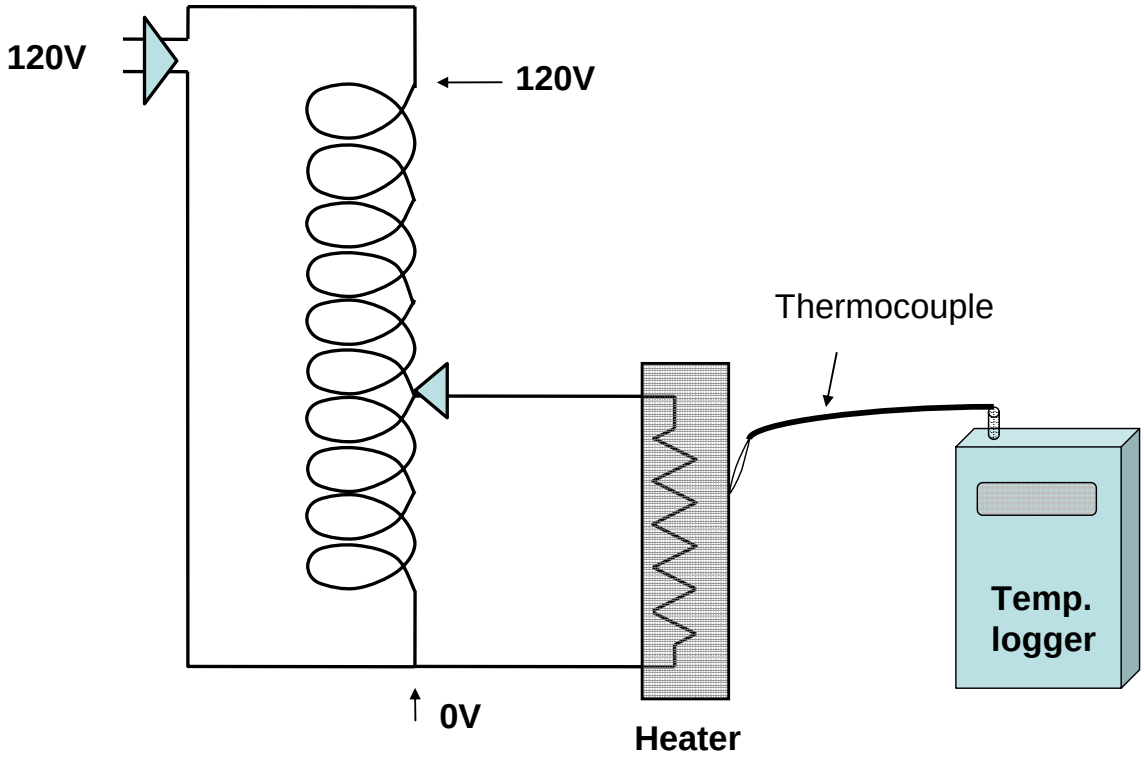

Figure 6 Diagram of the set-up for substrate heater which can go to 770°C at 120 V.

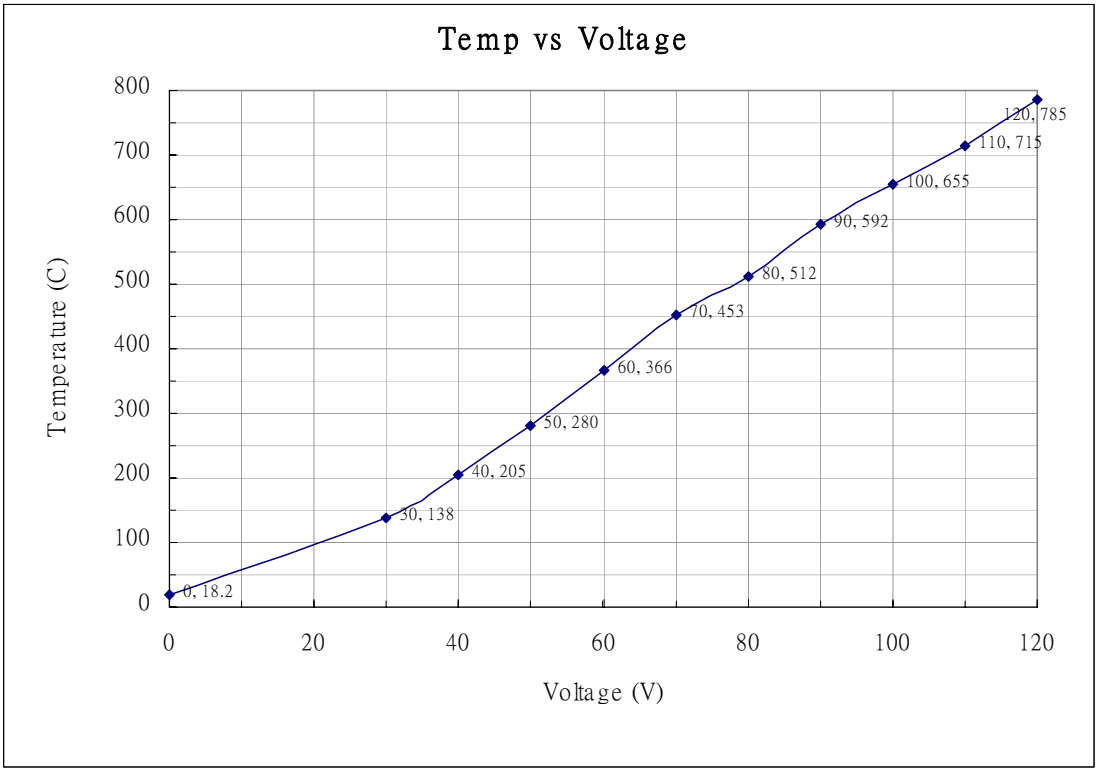

Figure 7 Temperature vs. voltage diagram on the substrate heater.

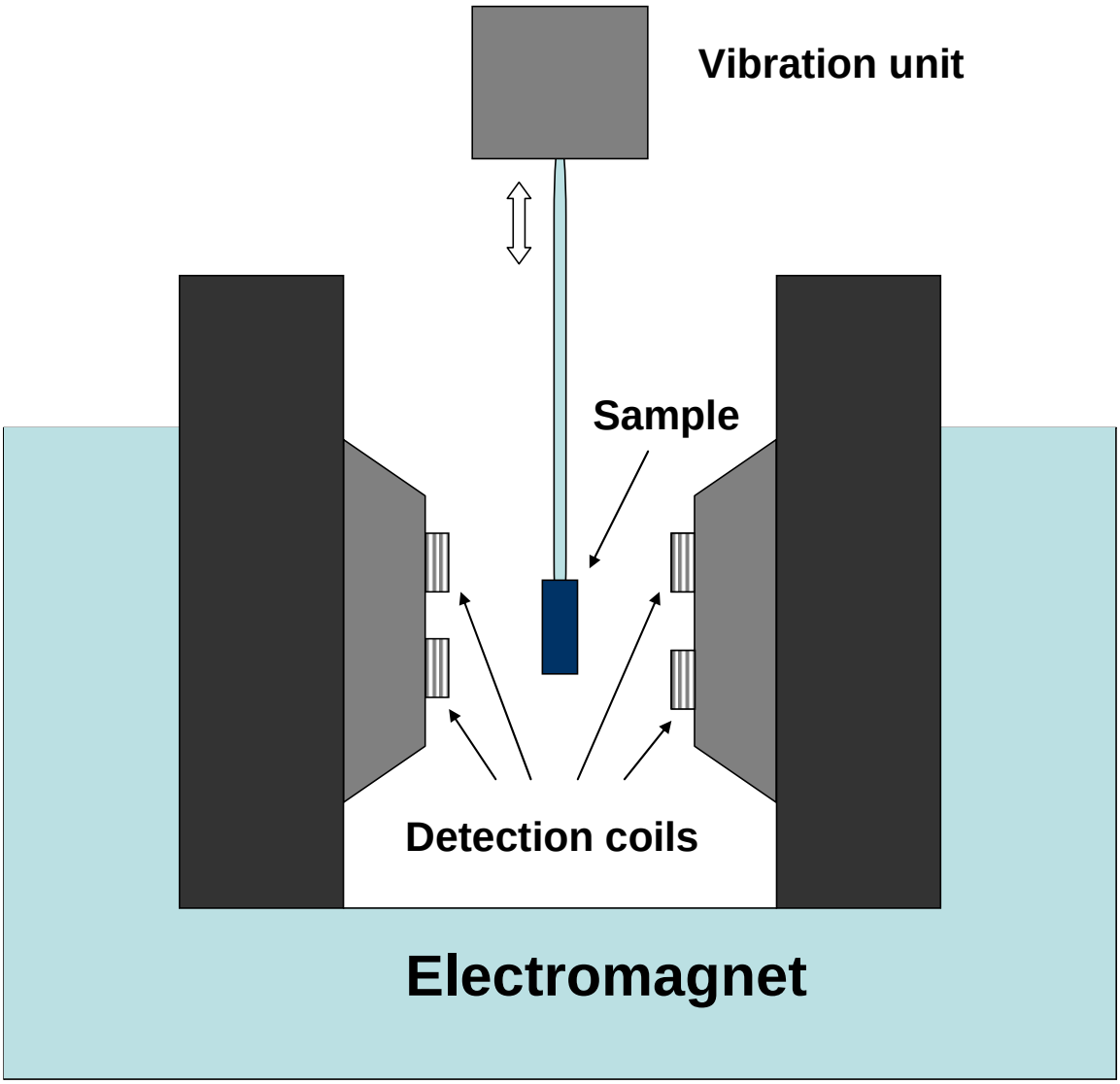

Figure 8 Schematic diagram of the VSM.

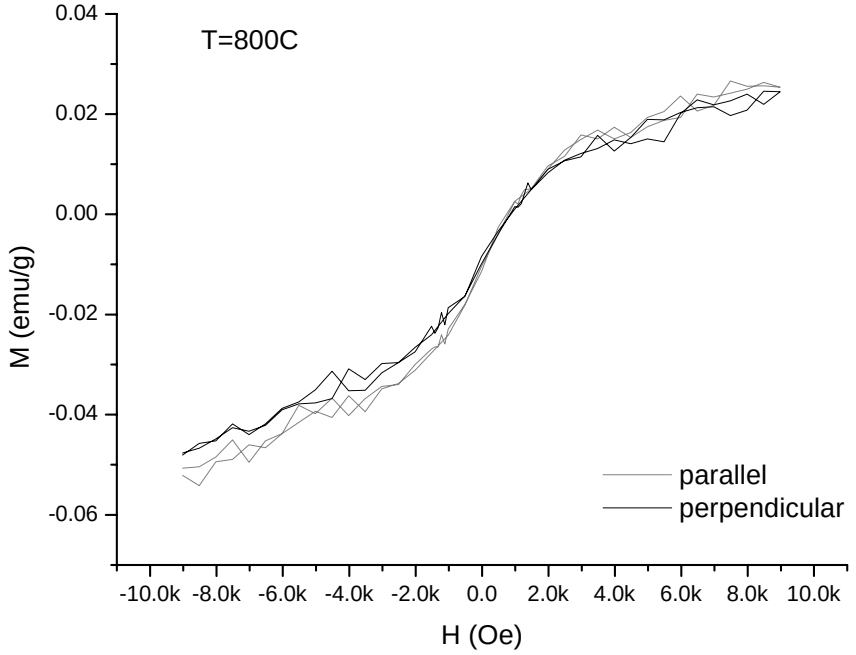

Figure 9 VSM hysteresis loops for the 34 mol% BaM film on sapphire (Al_2O_3)(0001) substrate heated at 800°C for 1hr.

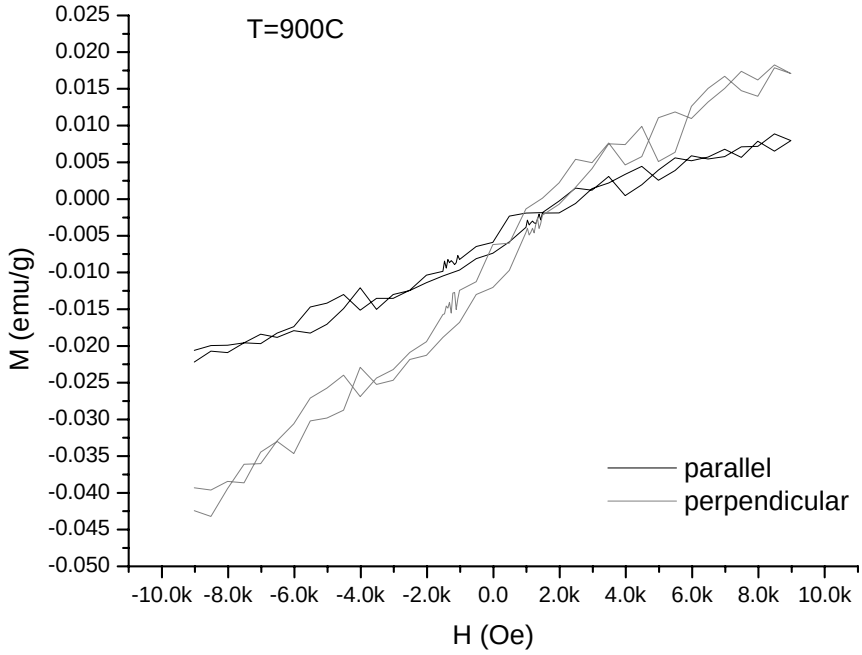

Figure 10 VSM hysteresis loops for the 34 mol% BaM film on sapphire (Al_2O_3)(0001) substrate heated at 900°C for 1hr.

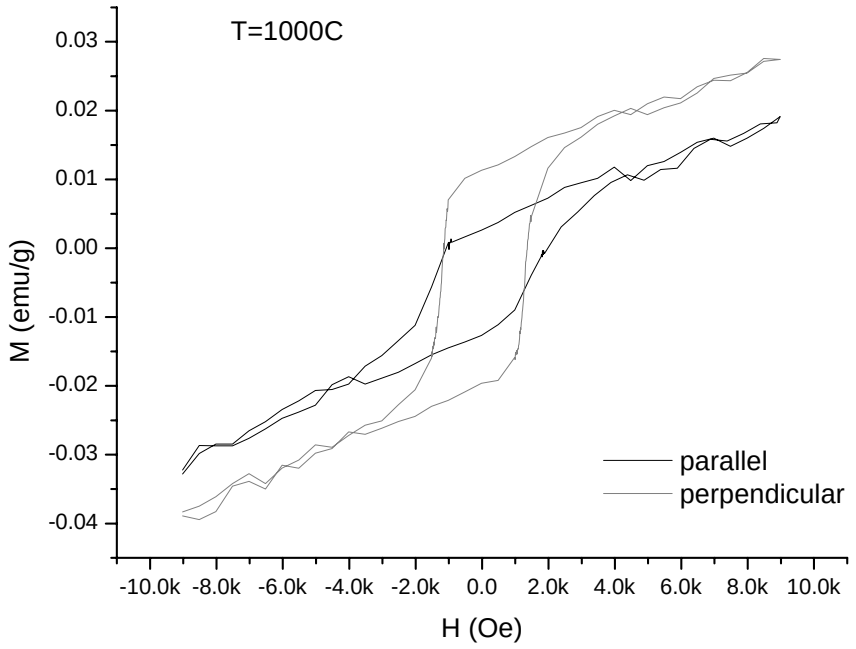

Figure 11 VSM hysteresis loops for the 34 mol% BaM film on sapphire (Al_2O_3)(0001) substrate heated at 1000°C for 1hr.

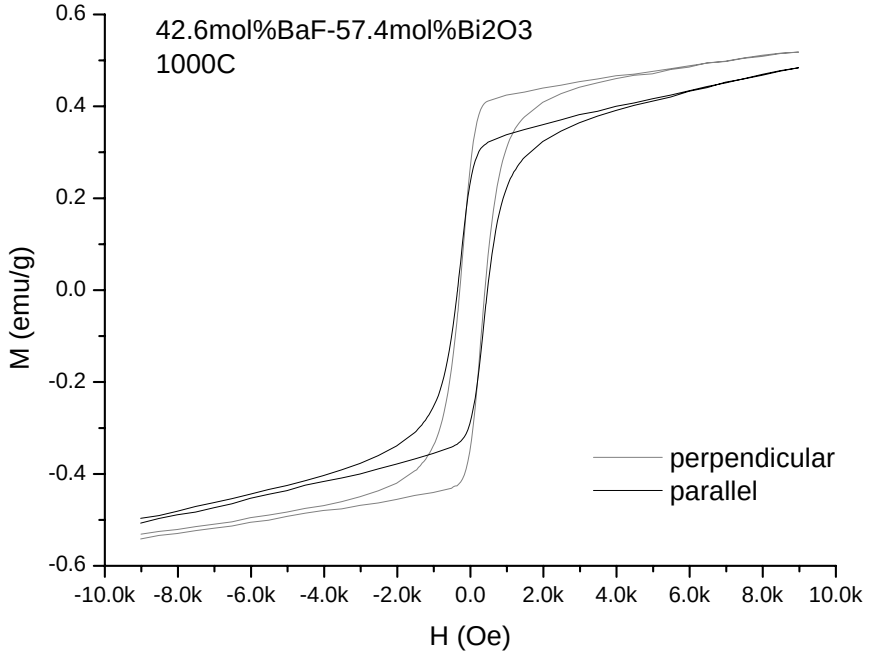

Figure 12 VSM hysteresis loops for 42.6 mol% BaM on sapphire (Al_2O_3)(0001) substrate heated at 1000°C for 1hr.

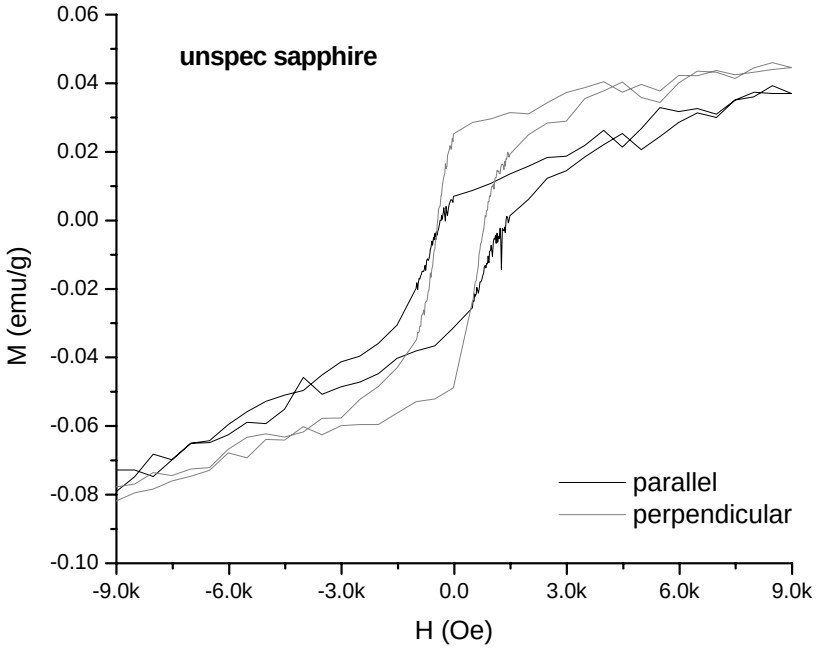

Figure 13 VSM hysteresis loops for the 34 mol% BaM film on unspecified sapphire (Al_2O_3) substrate heated at 1000°C for 1hr.

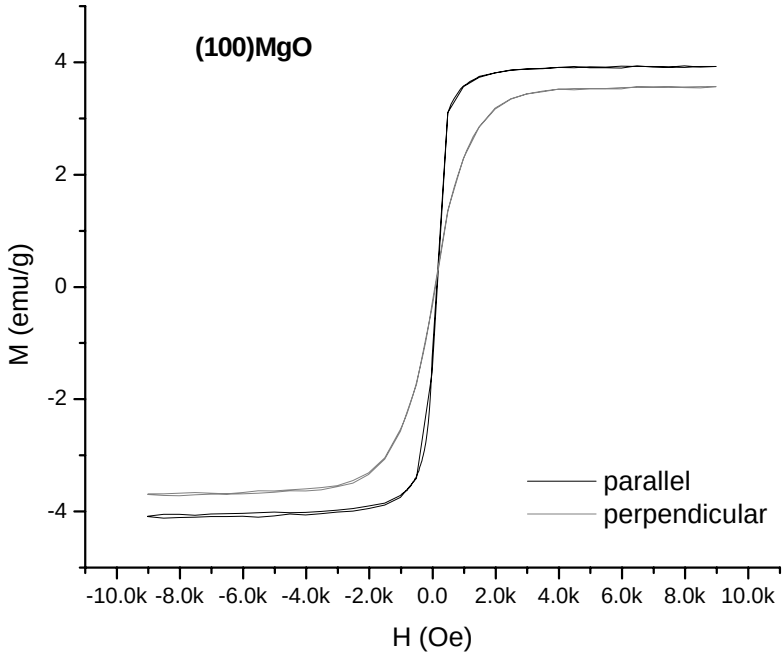

Figure 14 VSM hysteresis loops for the 34 mol% BaM film on (100)MgO substrate heated at 1000°C for 1hr.

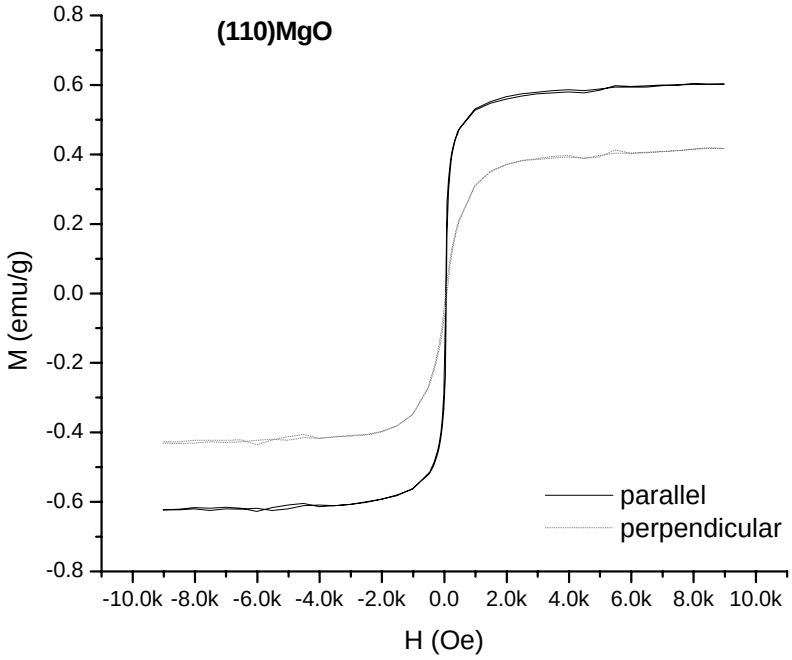

Figure 15 VSM hysteresis loops for the 34 mol% BaM film on (110) MgO substrate heated at 1000°C for 1hr.

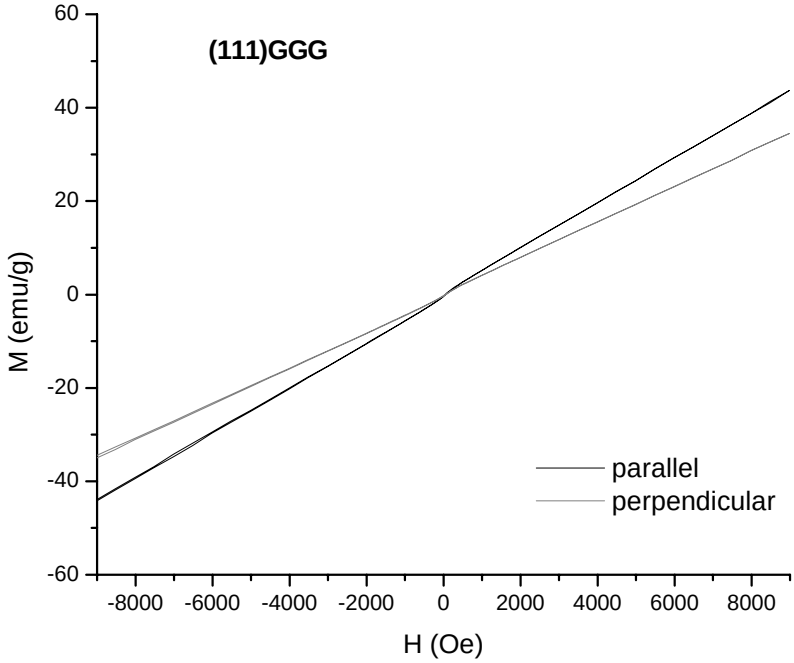

Figure 16 VSM hysteresis loops for the 34 mol% BaM film on (111) GGG substrate heated at 1000°C for 1hr.

Coercivity (Oe)	**C-axis Al_2O_3**	**Unspec. Al_2O_3**	**(100)MgO**	**(110)MgO**	**(111)GGG**
Parallel	1528.372	880.603	9.712	9.17	9.071
Perpendicular	1258.018	626.814	9.757	19.42	8.836

Table 4 Coercive filed of the 34 mol% BaM films heated at 1000 °C for 1 hr on different substrates.

Magnetization (emu/g)	**C-axis Al_2O_3**	**Unspec. Al_2O_3**	**(100)MgO**	**(110)MgO**
Parallel	0.0257	0.059	4.027	0.616
Perpendicular	0.033	0.064	3.647	0.427

Table 5 Magnetization of the 34 mol% BaM films heated at 1000 °C for 1 hr on different substrates.

	Substrates	M_{9000} (emu)	M_{2000} (emu)	**Slope** (memu/Oe)	**Anisotropy**
34 mol% BaM	Unspc. Al_2O_3 ⊥	3.7002E-4	2.5830E-4	1.60E-05	1.56 ($\mathbf{S}_{//}$ / $\mathbf{S}_{\perp}$)
	Unspc. Al_2O_3 //	3.0654E-4	1.3136E-4	2.50E-05	
	c-axis Al_2O_3 ⊥	6.6428E-4	3.8942E-4	3.93E-05	1.04 ($\mathbf{S}_{//}$ / $\mathbf{S}_{\perp}$)
	c-axis Al_2O_3 //	4.6302E-4	1.7570E-4	4.10E-05	
	(100)MgO ⊥	6.4184E-3	6.3384E-3	1.60E-05	3.15 ($\mathbf{S}_{\perp}$ / $\mathbf{S}_{//}$)
	(100)MgO //	7.0666E-3	7.0412E-3	5.08E-06	
	(110)MgO⊥	2.7494E-3	2.4512E-3	4.26E-05	1.22 ($\mathbf{S}_{\perp}$ / $\mathbf{S}_{//}$)
	(110)MgO //	3.9808E-3	3.7362E-3	3.49E-05	
42.6 mol% BaM	c-axis Al_2O_3 ⊥	8.8600E-3	6.9934E-3	2.67E-04	1.47 ($\mathbf{S}_{//}$ / $\mathbf{S}_{\perp}$)
	c-axis Al_2O_3 //	8.2754E-3	5.5276E-3	3.93E-04	

Table 6 Anisotropy of BaM films on different substrates. M_{9000} is the magnetization value at 9000 Oe and M_{2000} is the magnetization value at 2000 Oe.

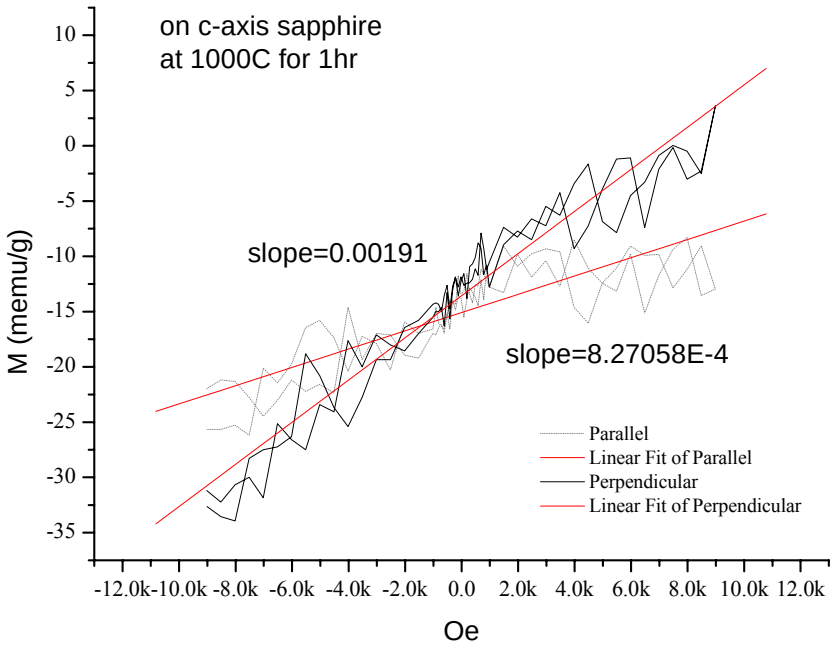

Figure 17 VSM hysteresis loops for the 2.7mol% $SrFe_{12}O_{19}$ + 97.3mol% Bi_2O_3 film on c-axis sapphire heated at 1000°C for 1hr.

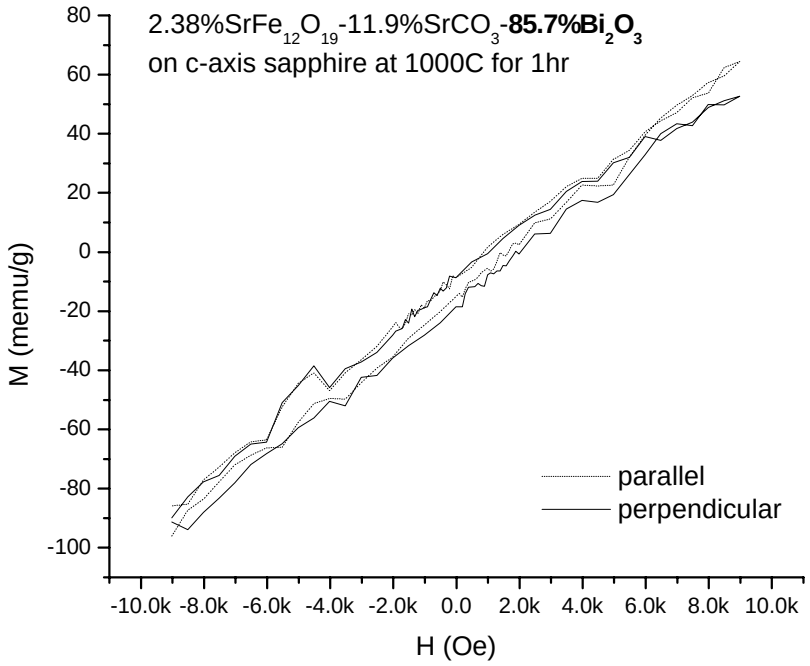

Figure 18 VSM hysteresis loops for the 2.38mol% $SrFe_{12}O_{19}$+11.9% $SrCO_3$+ 85.7mol% Bi_2O_3 film on c-axis sapphire heated at 1000°C for 1hr

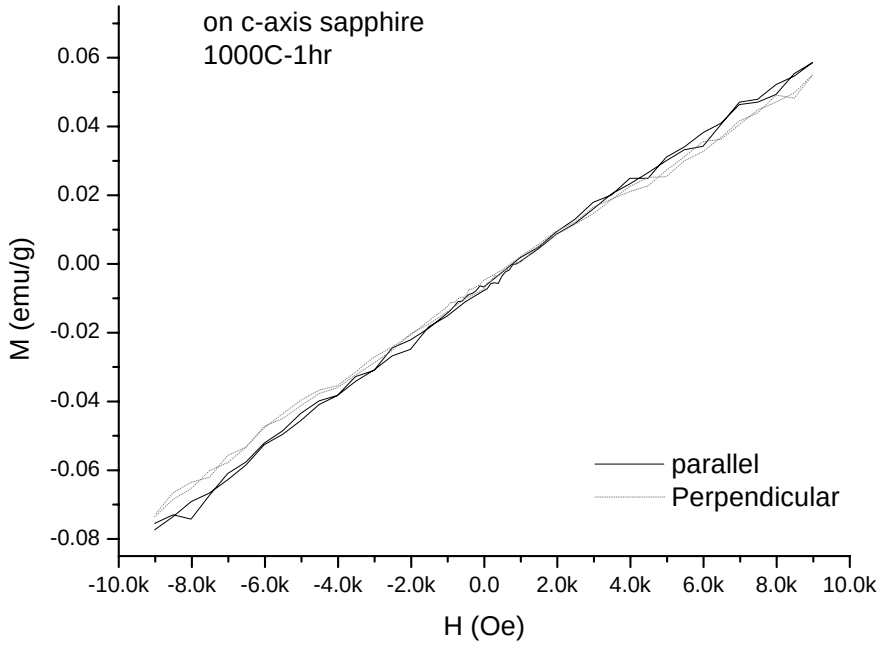

Figure 19 VSM hysteresis loops for the 4.16mol%$SrFe_{12}O_{19}$ +20.84mol%$SrCO_3$ + 75mol%Bi_2O_3 film on c-axis sapphire heated at 1000°C for 1hr

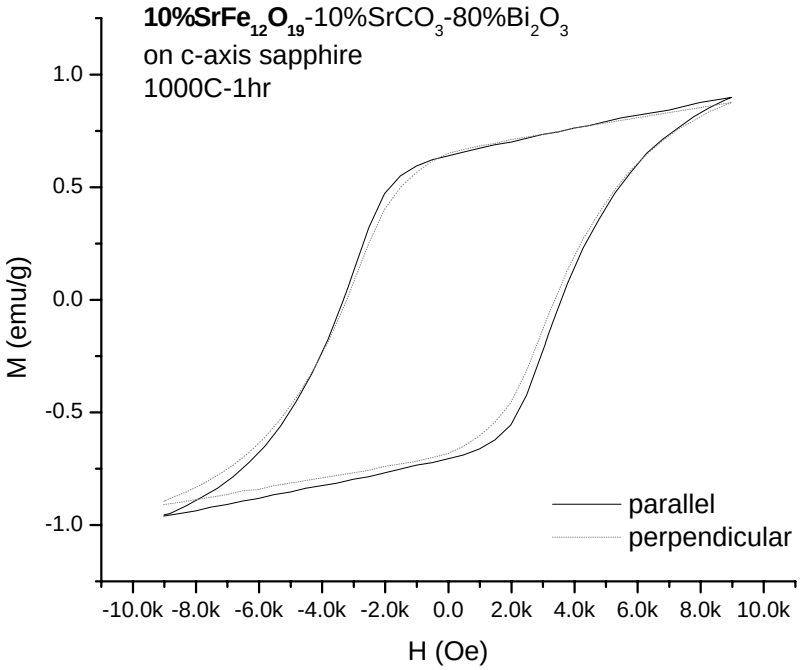

Figure 20 VSM hysteresis loops for the 10mol% $SrFe_{12}O_{19}$ +10mol%$SrCO_3$ + 80mol%Bi_2O_3 film on c-axis sapphire heated at 1000°C for 1hr.

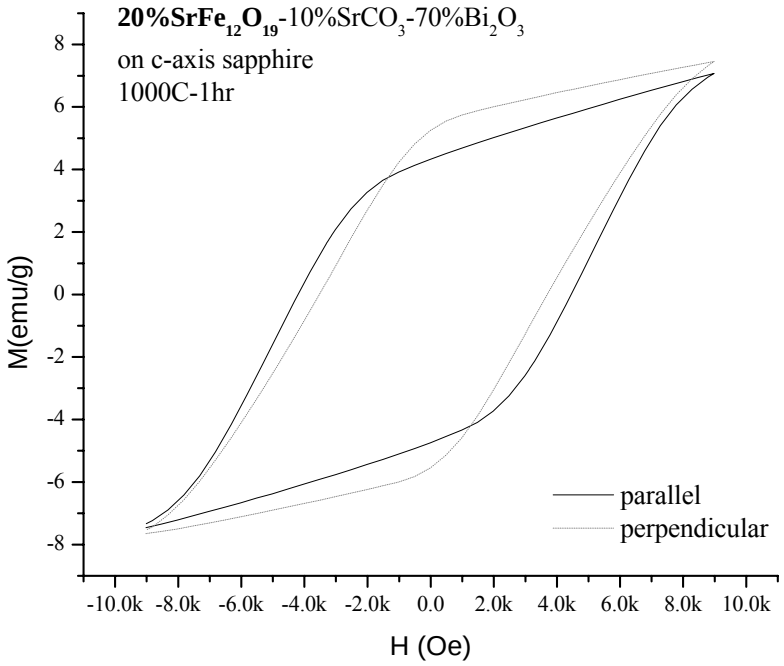

Figure 21 VSM hysteresis loops for the 20mol% $SrFe_{12}O_{19}$ +10mol%$SrCO_3$ + 70mol%Bi_2O_3 film on c-axis sapphire heated at 1000°C for 1hr.

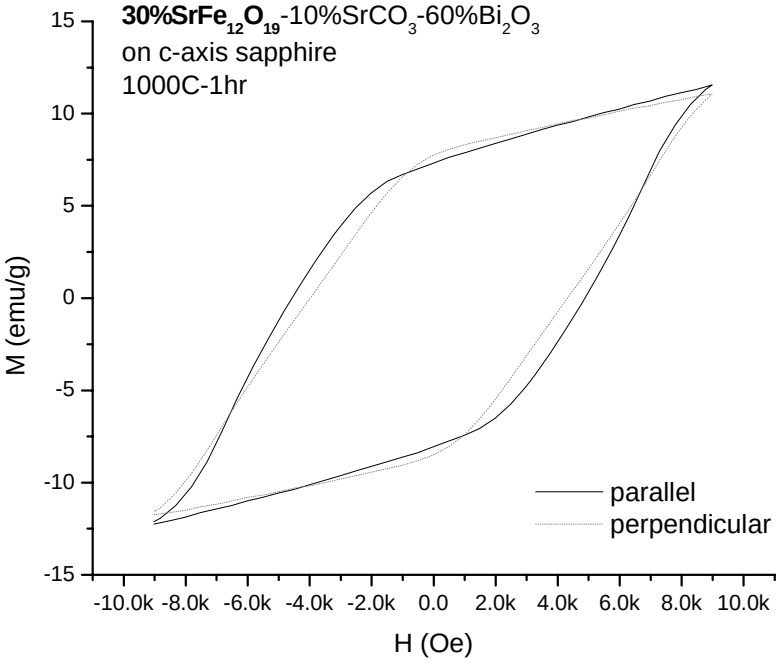

Figure 22 VSM hysteresis loops for the 30mol% $SrFe_{12}O_{19}$ +10mol%$SrCO_3$ + 60mol%Bi_2O_3 film on c-axis sapphire heated at 1000°C for 1hr.

Coercivity (Oe)	**10%$SrFe_{12}O_{19}$**	**20%$SrFe_{12}O_{19}$**	**30%$SrFe_{12}O_{19}$**
Parallel	3451.760	4324.521	4722.152
Perpendicular	3298.103	3609.292	4152.660

Table 7 Coercive field of the strontium ferrite films on c-axis sapphire heated at 1000 °C for 1 hr.

Magnetization(emu/g)	**10%$SrFe_{12}O_{19}$**	**20%$SrFe_{12}O_{19}$**	**30%$SrFe_{12}O_{19}$**
Parallel	0.929	7.270	11.881
Perpendicular	0.894	7.572	11.431

Table 8 Magnetization of the strontium ferrite films on c-axis sapphire heated at 1000 °C for 1 hr.

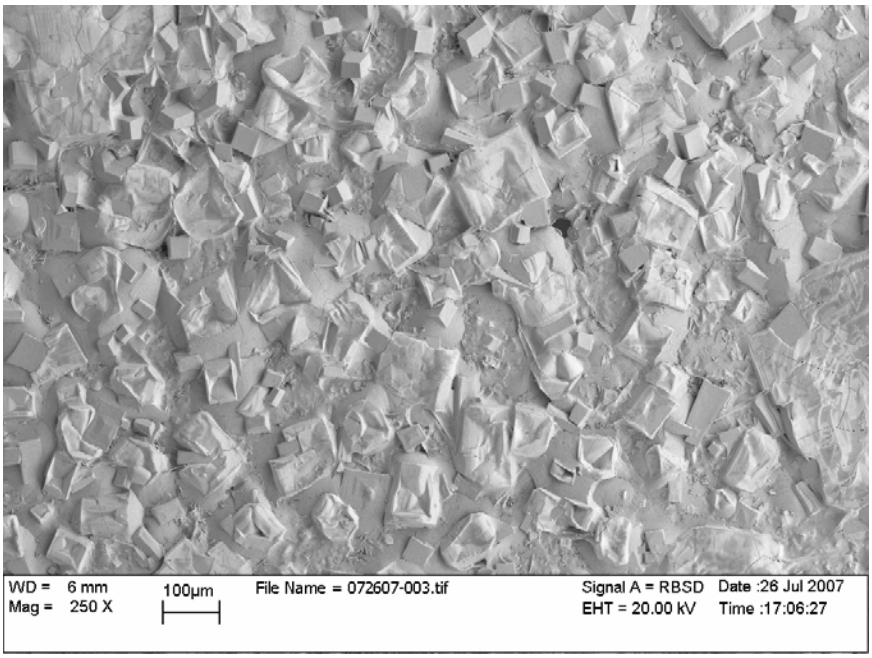

(a)

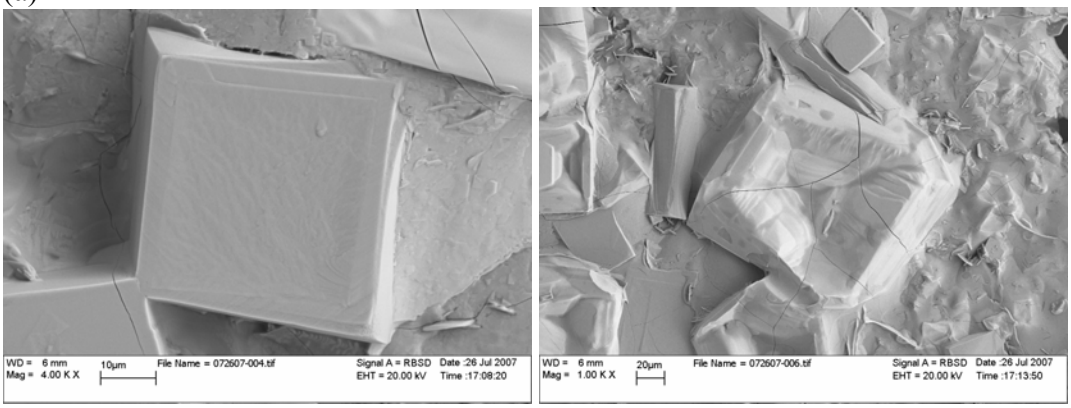

(b) (c)

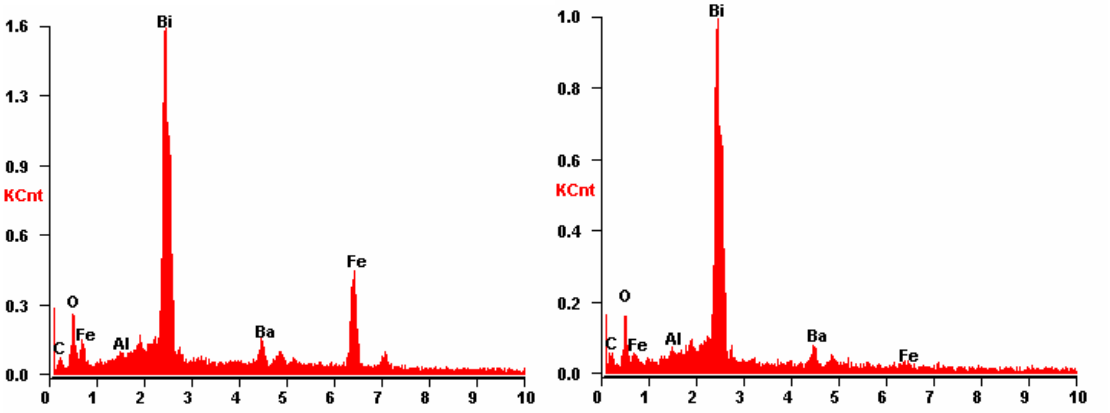

(d) (e)

Figure 23 SEM images and EDAX spectrums of the BaM film on sapphire (Al_2O_3)(0001) substrate heated at 800°C for 1hr.

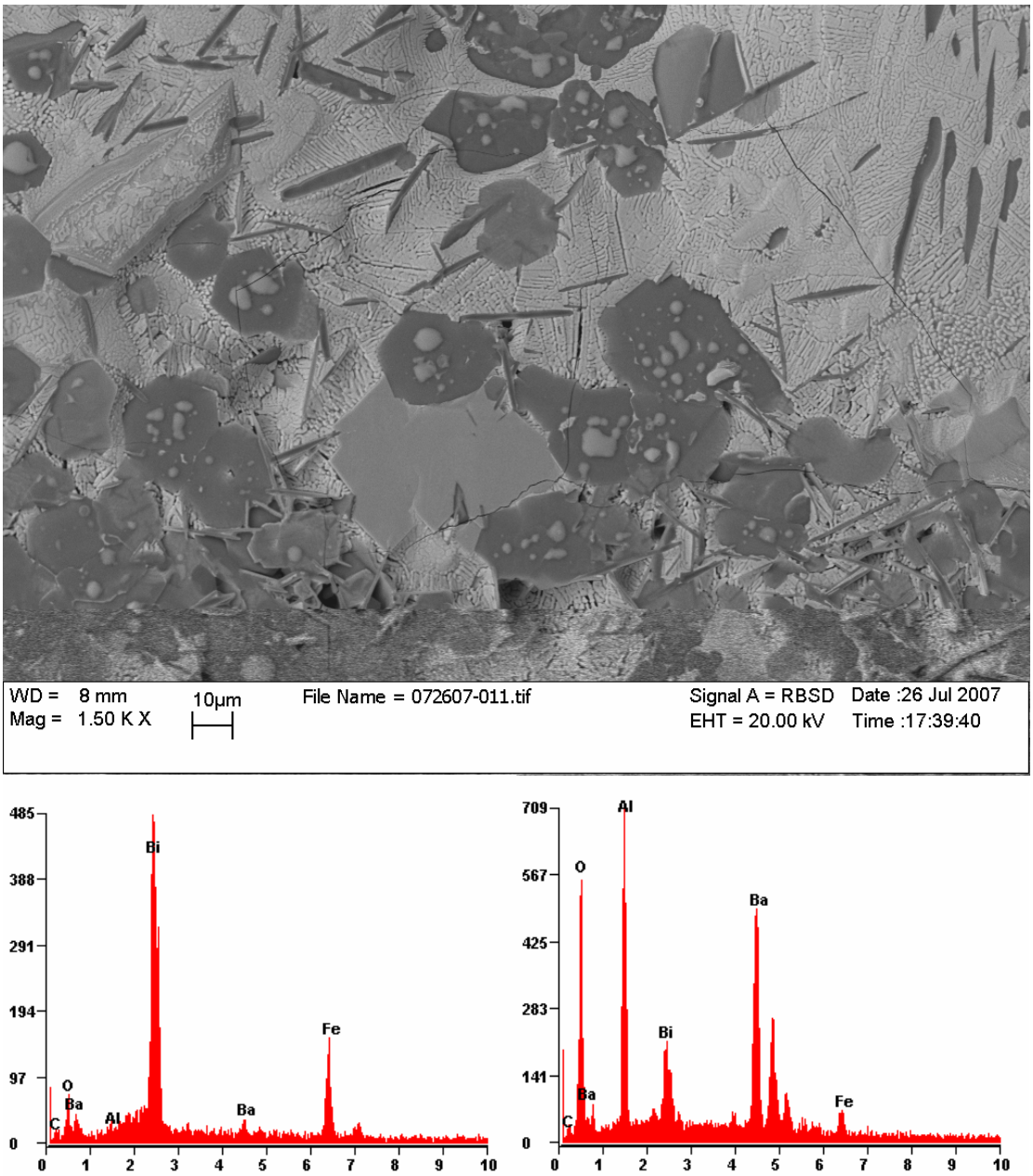

Figure 24 (a)SEM images of the 34 mol% BaM film on sapphire (Al_2O_3)(0001) substrate heated at 900°C for 1hr.(b)EDAX spectrum on square crystals (c) EDAX spectrum on hexagons.

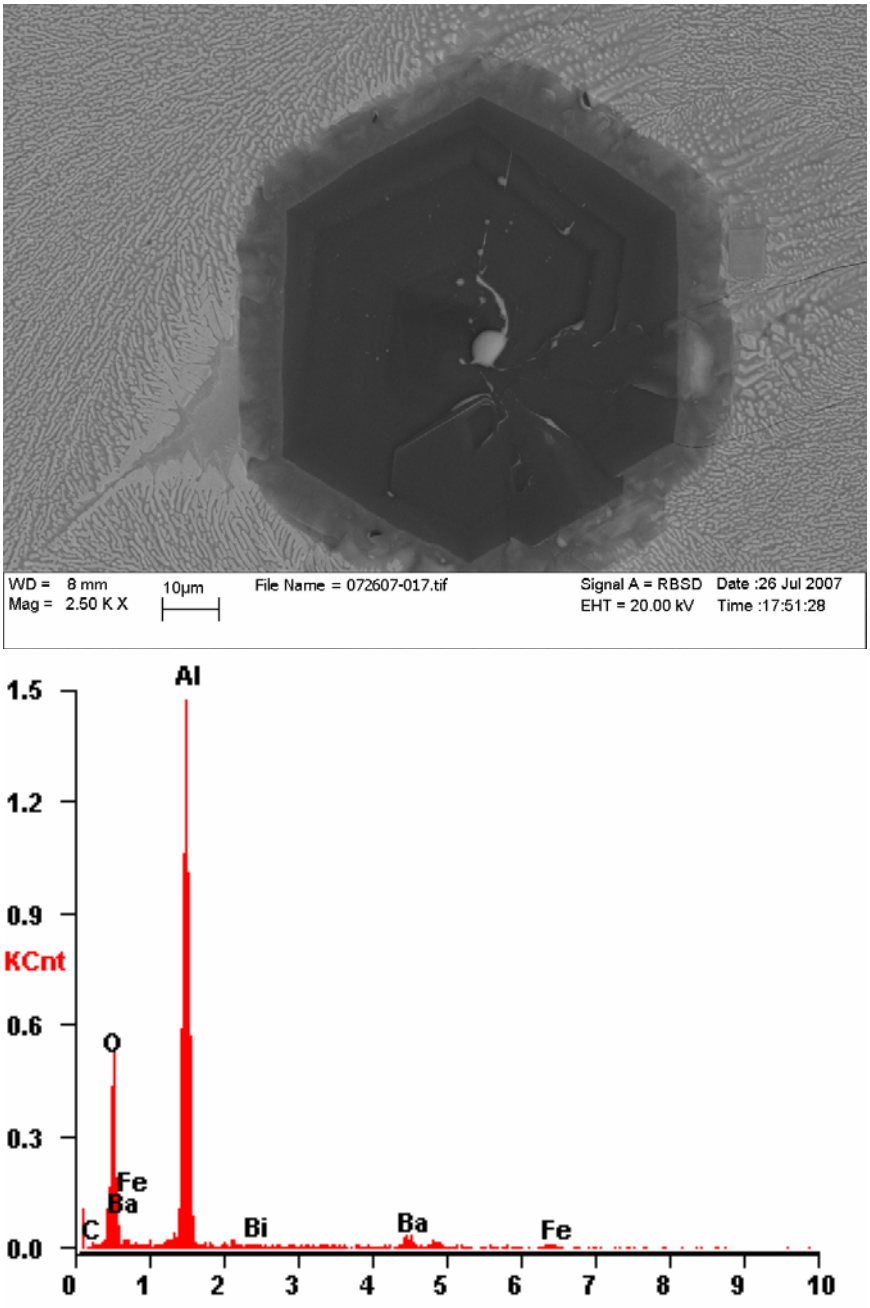

Figure 25 (a) SEM images and (b) EDAX spectrum of the 34 mol% BaM film on sapphire (Al_2O_3)(0001) substrate heated at 1000°C for 1hr.

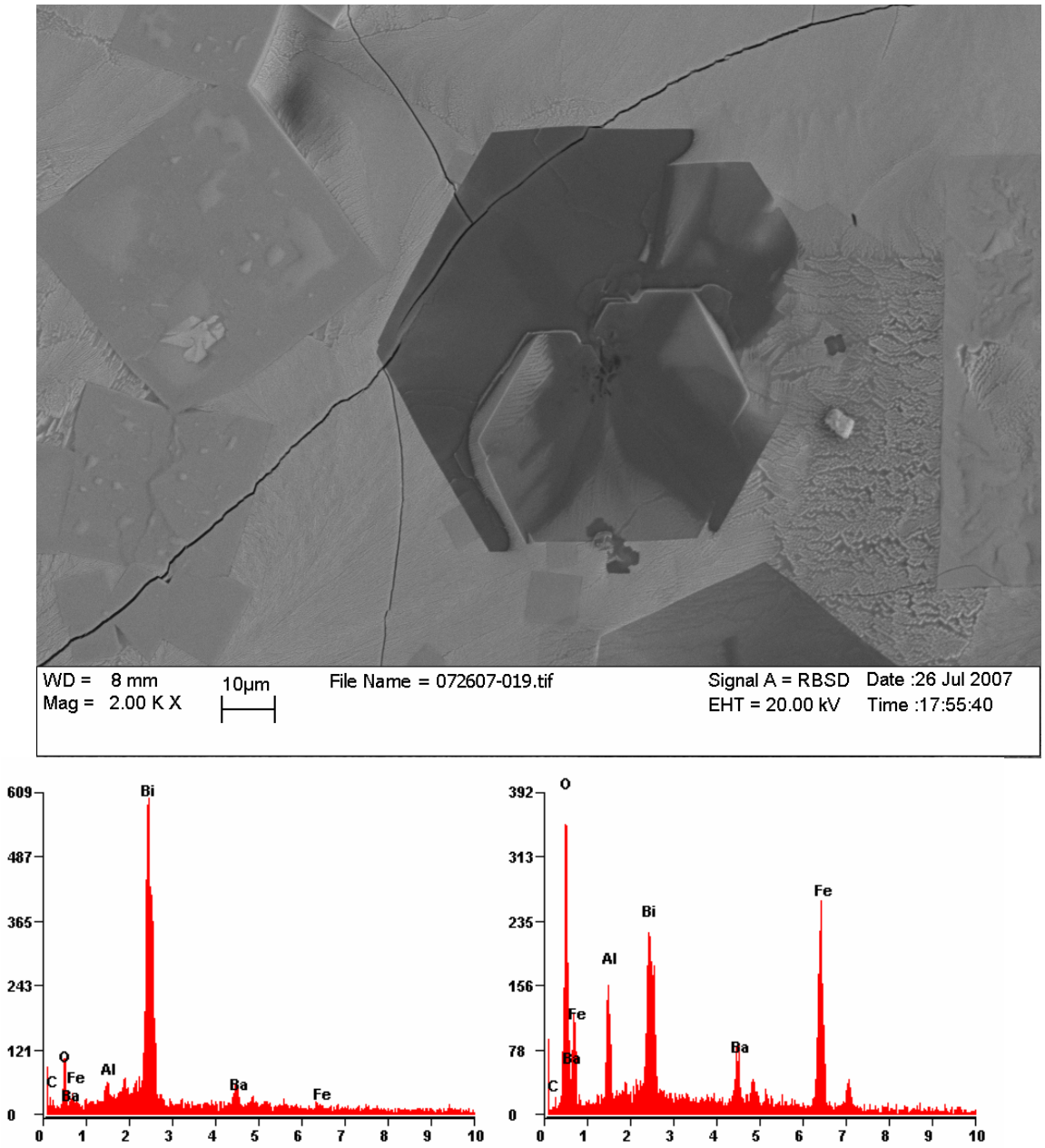

Figure 26 (a) SEM images of the 42.6 mol%BaM film on sapphire (Al_2O_3)(0001) substrate heated at 1000°C for 1hr. (b) EDAX spectrum for square crystals. (c) EDAX spectrum for hexagons.

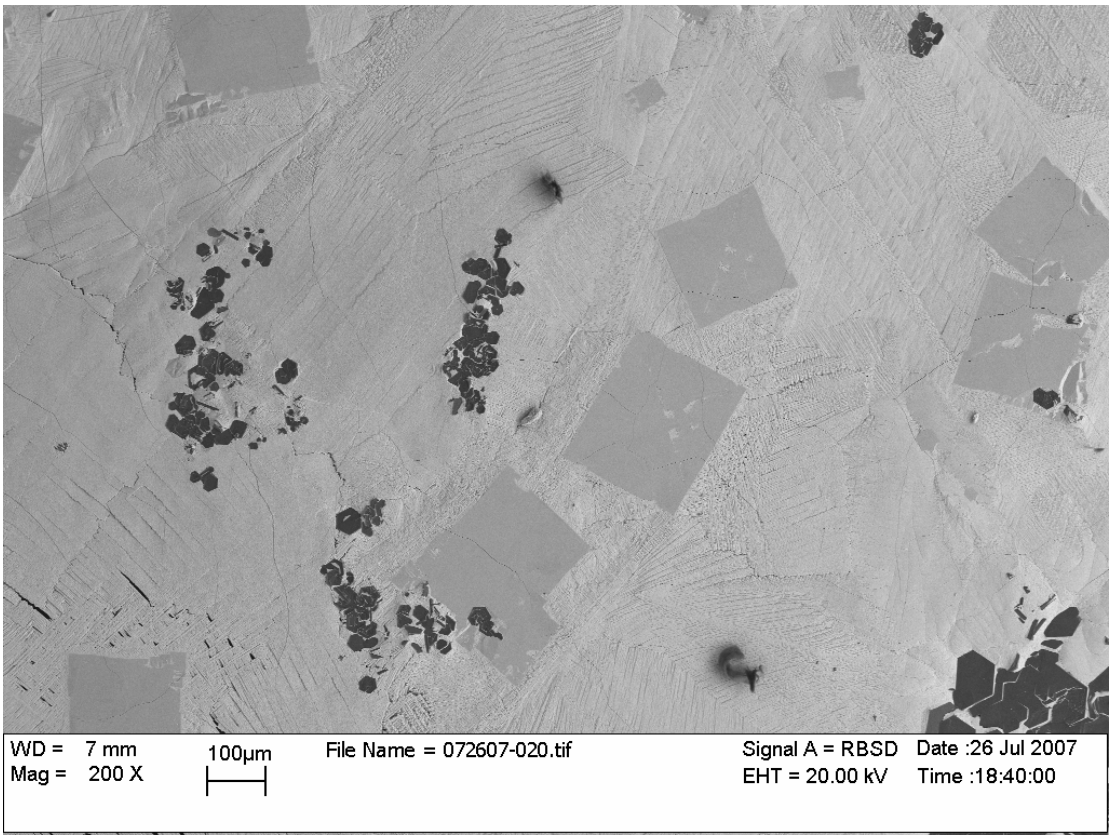

Figure 27 (a) SEM images of the 4.16 mol% SrM film on sapphire (Al2O3)(0001) substrate heated at 1000°C for 1hr. (b) EDAX spectrum for square crystals. (c) EDAX spectrum for hexagons.

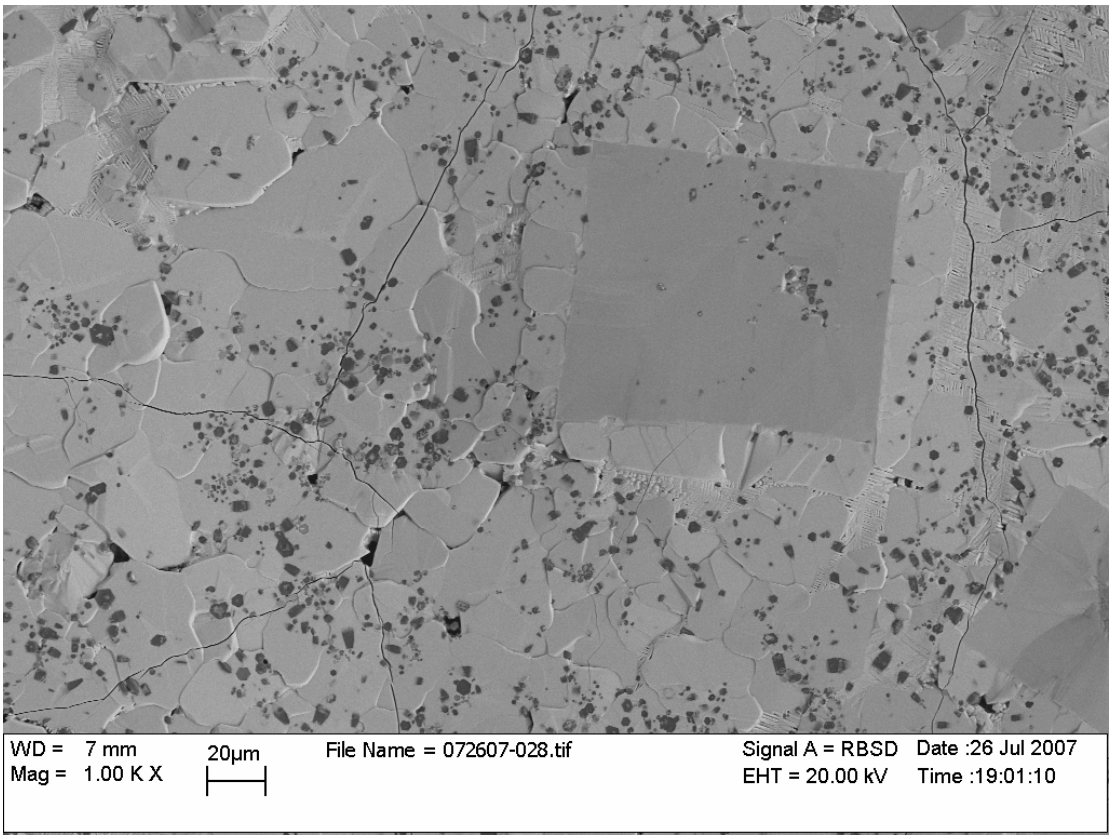

(a)

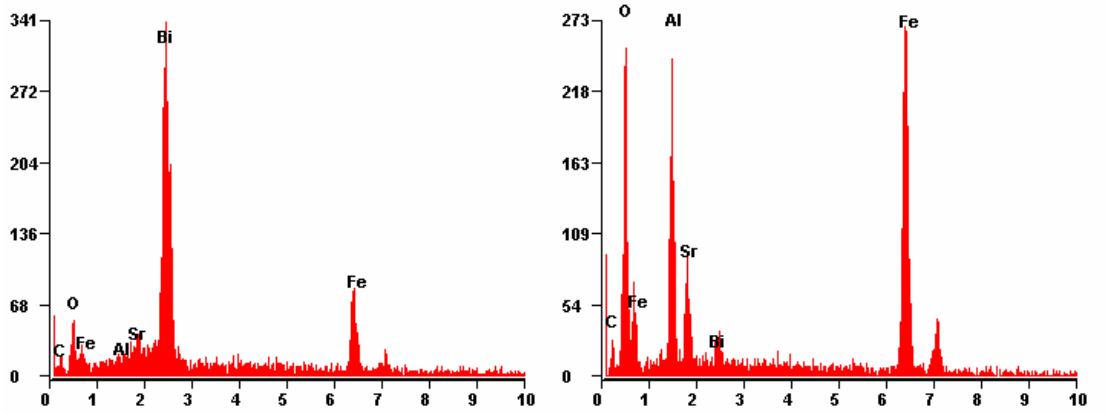

(b) (c)

Figure 28 (a) SEM images of the 10 mol% SrM film on sapphire (Al_2O_3)(0001) substrate heated at 1000°C for 1hr. (b) EDAX spectrum for square crystals. (c) EDAX spectrum for hexagons.

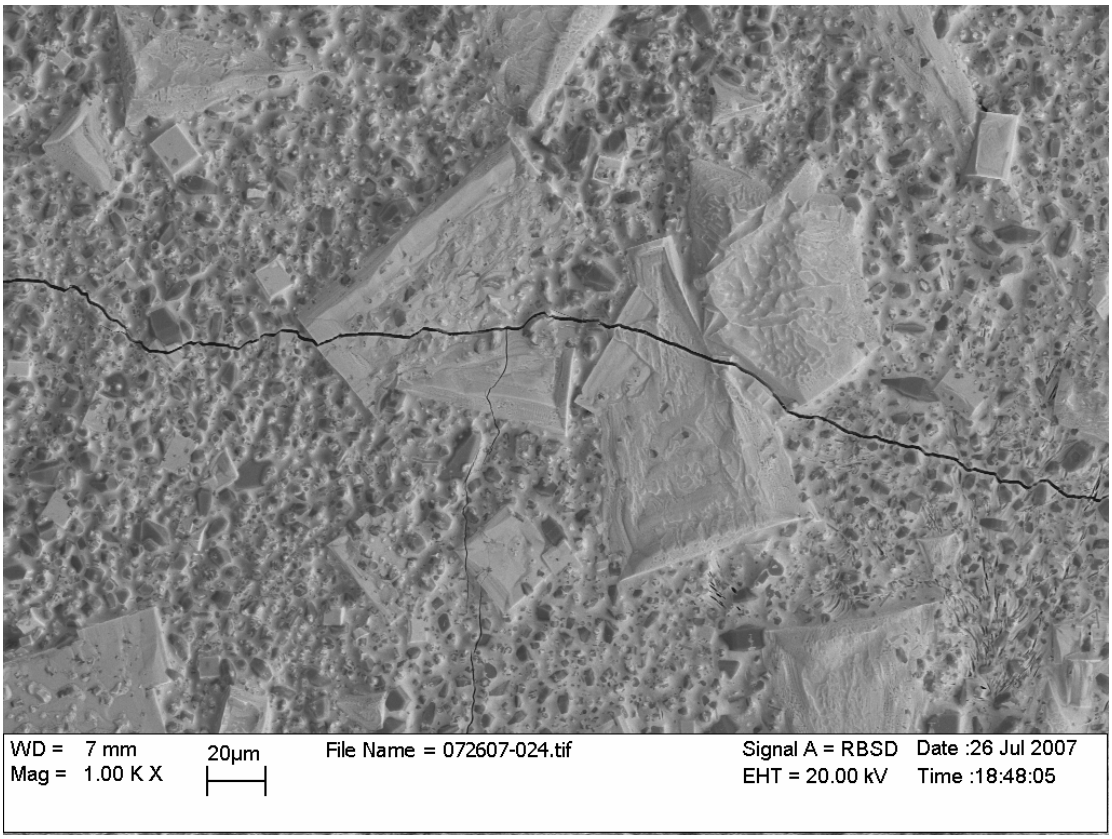

(a)

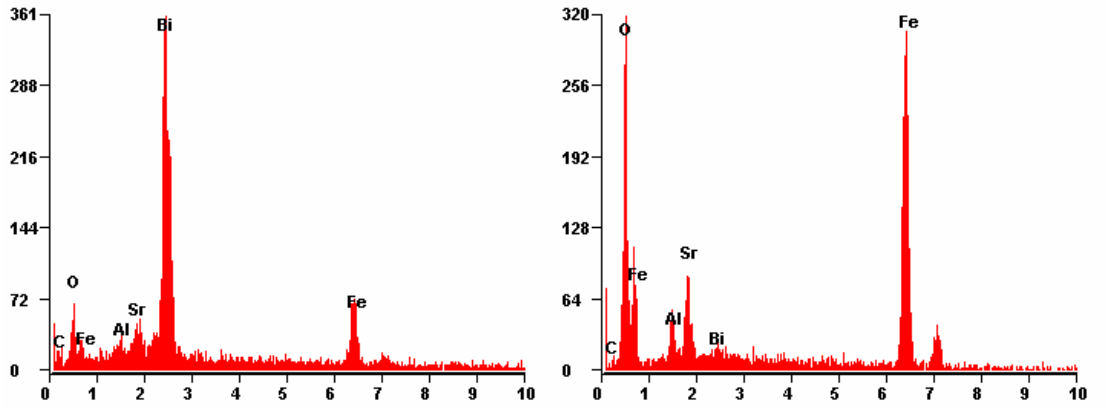

(b) (c)

Figure 29 (a) SEM images of the 20 mol% SrM film on sapphire (Al_2O_3)(0001) substrate heated at 1000°C for 1hr. (b) EDAX spectrum for square crystals. (c) EDAX spectrum for dark particles.

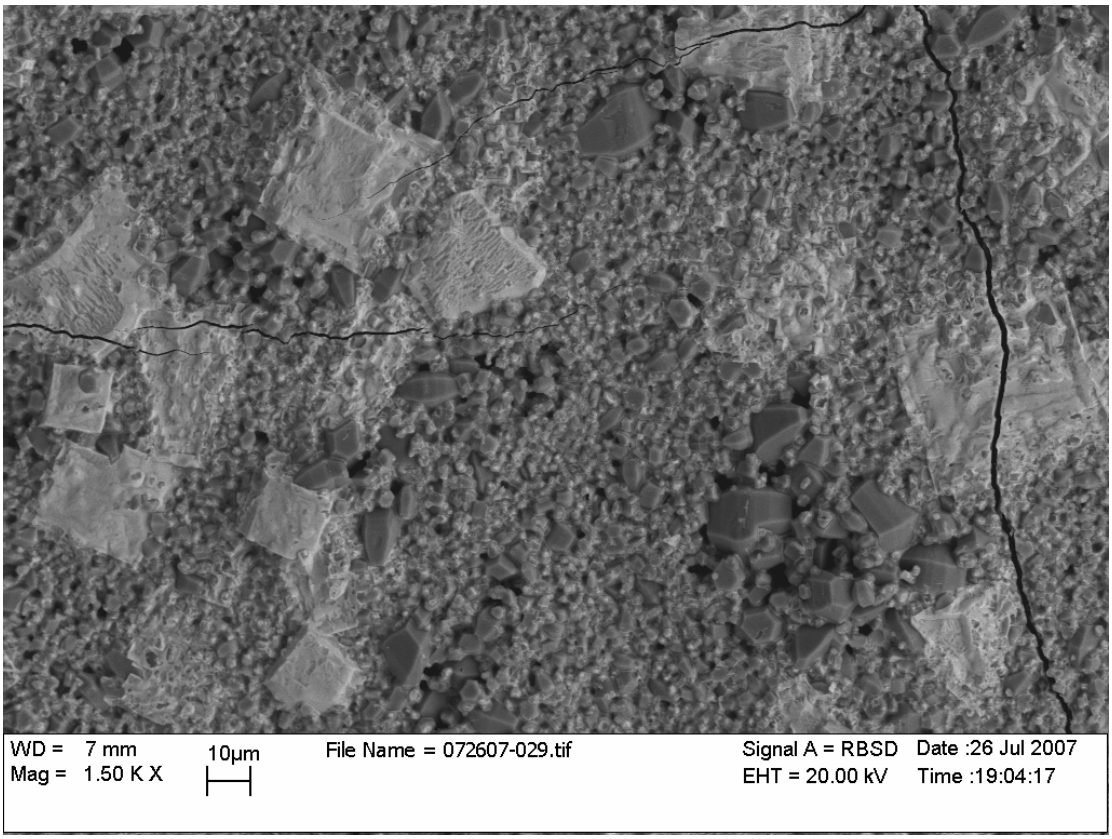

(a)

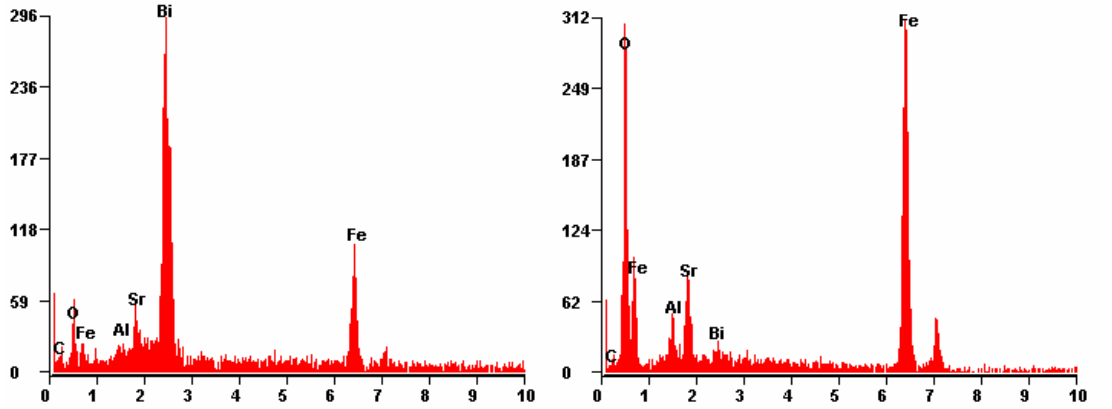

(b) (c)

Figure 30 (a) SEM images of the 30 mol% SrM film on sapphire (Al_2O_3)(0001) substrate heated at 1000°C for 1hr. (b) EDAX spectrum for square crystals. (c) EDAX spectrum for dark particles.

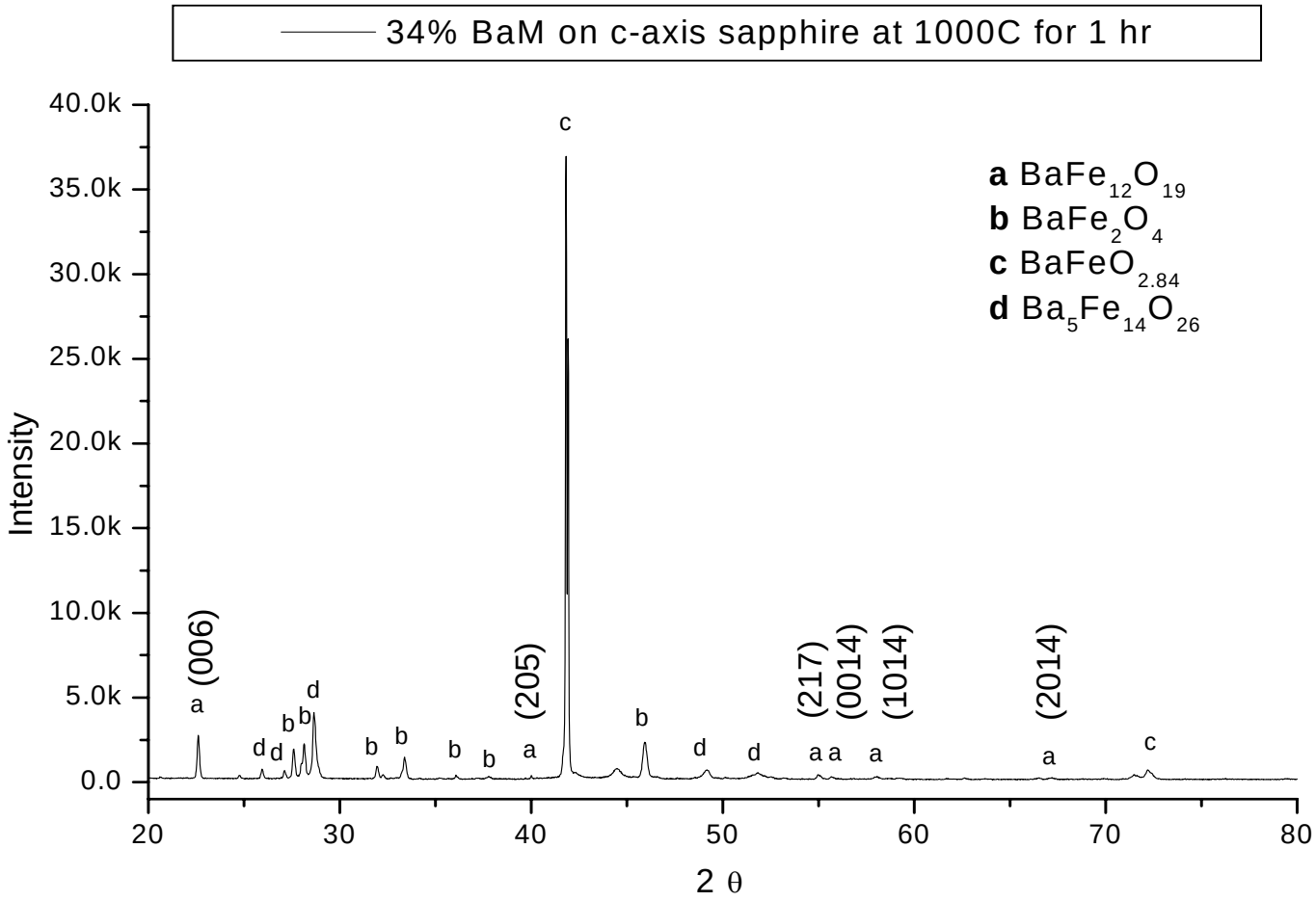

Figure 31 XRD spectrum on 34 mol% BaM on c-axis Al_2O_3 substrate heated at 1000°C for 1hr.

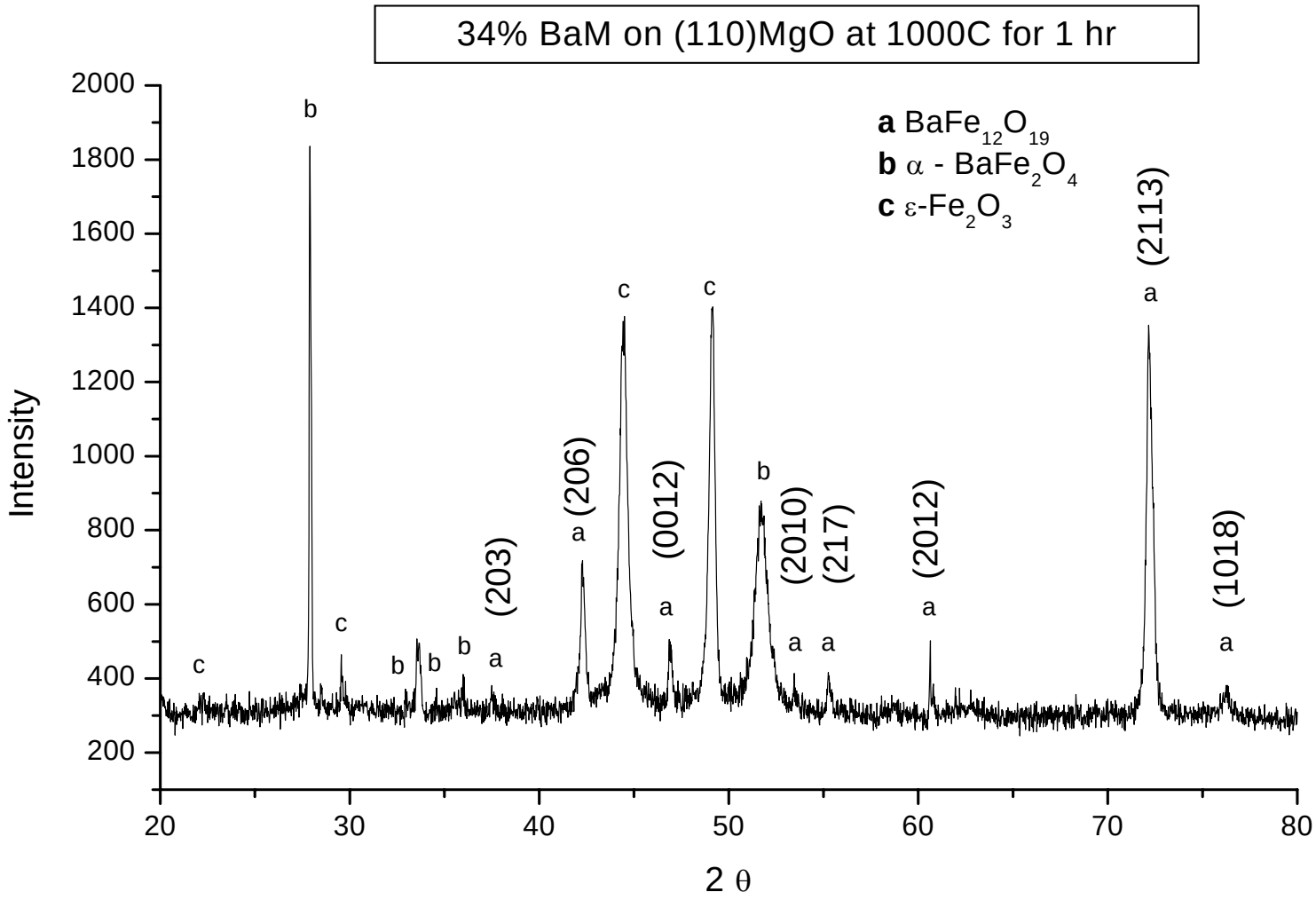

Figure 32 XRD spectrum on 34 mol% BaM on (110) MgO substrate heated at 1000°C for 1hr.

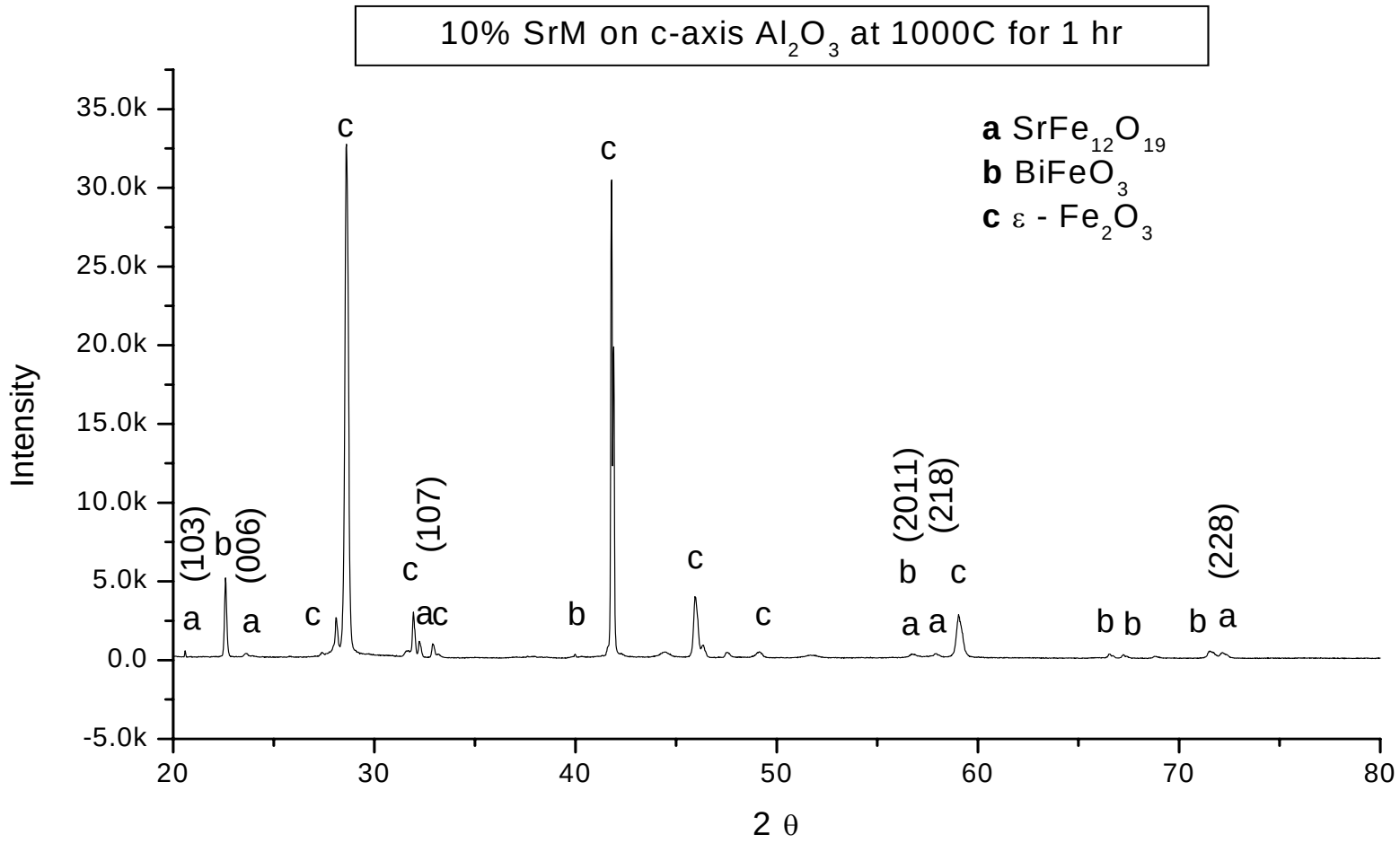

Figure 33 XRD spectrum on 10 mol% SrM on c-axis Al_2O_3 substrate heated at 1000°C for 1hr.

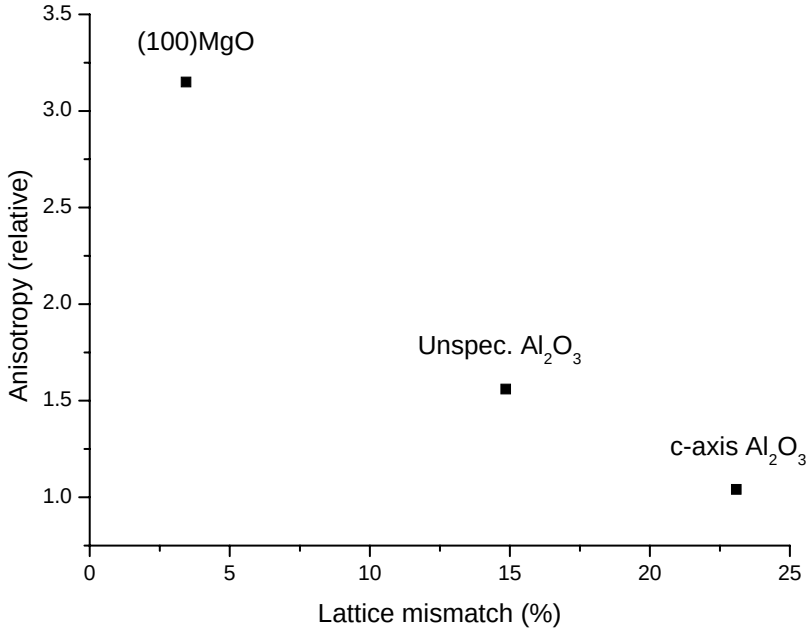

Figure 34 Lattice mismatch dependence of anisotropy in BaM films on different substrates.

SrM	M_{9000} (emu/g)	M_{2000} (emu/g)	Slope (memu/Oe)	Anisotropy ($\mathbf{S}_{//}$ / $\mathbf{S}_{\perp}$)
10% //	0.89831	0.70056	0.02825	1.21
10% ⊥	0.87571	0.71186	0.023407143	
20% //	7.07576	5.01515	0.294372857	1.41
20% ⊥	7.46212	6	0.208874286	
30% //	11.5625	8.375	0.455357143	1.34
30% ⊥	11.0625	8.6875	0.339285714	

Table 9 Anisotropy of the different ratios of SrM films on c-axis Al_2O_3 substrates. M_{9000} is the magnetization value at 9000 Oe and M_{2000} is the magnetization value at 2000 Oe.

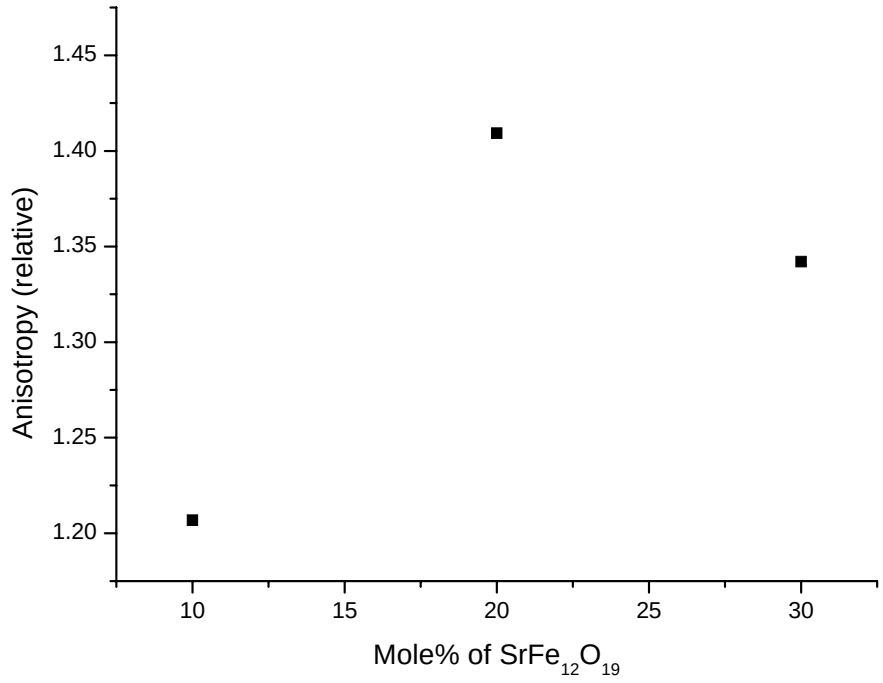

Figure 35 Anisotropy of the different ratios of SrM films on c-axis Al_2O_3 substrates.

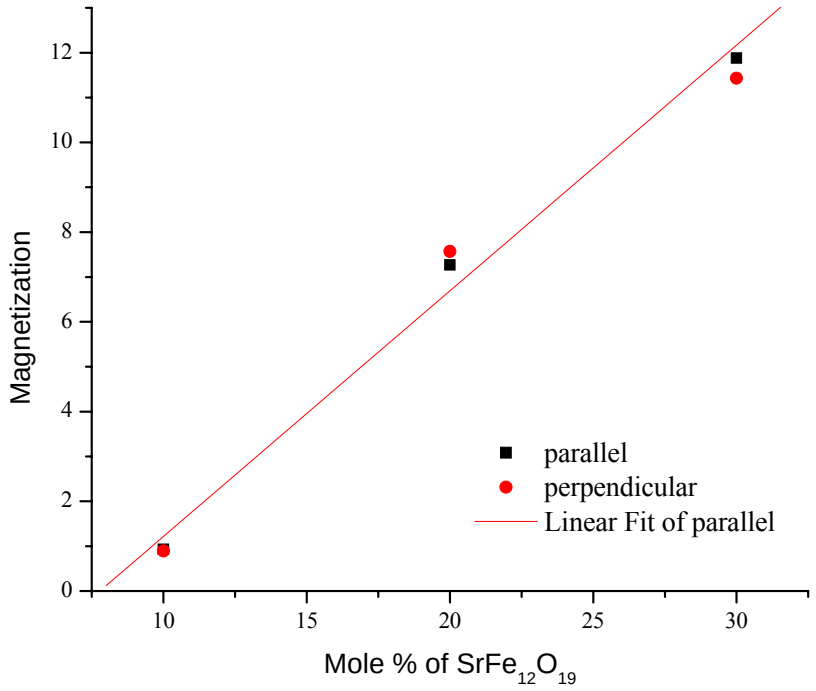

Figure 36 Composition dependence of magnetization in SrM films.

Reference

1. Fang, H.C. and C.K. Ong, *Epitaxy barium ferrite thin films on LiTaO3 substrate.* Journal of Applied Physics, 1999. **86**(4): p. 2191.
2. Harris, V.G., et al., *Ba-hexaferrite films for next generation microwave devices (invited).* Journal of Applied Physics, 2006. **99**(8): p. 08M911.
3. Nicholson, D.B., *Hexagonal Ferrites for Millimeter-Wave Apllications.* Hewlett-Packard journal, 1990. **41**(5): p. 59-61.
4. O'Handley, R.C., *Modern Magnetic Materials: Principles and Applications*. 2000: John Wiley & Sons.
5. Dorsey, P.C., et al., *Oriented barium hexaferrite thick films grown on c-plane andm-plane sapphire substrates,* IEEE Transactions on Magnetics, 1994. **30**: p. 4512-4517.
6. Ramamurthy Acharya, B., et al., *Preparation and magnetic properties of strontium ferrite thin films.* IEEE Transactions on Magnetics, 1993. **29**(6): p. 3370-3372.
7. Garca, T., et al., *Textured strontium ferrite thin films grown by PLD.* Materials Letters, 2001. **49**: p. 294-298.
8. Koleva, M.E., et al., *Sr-ferrite thin films grown on sapphire by pulsed laser deposition.* Applied Surface Science, 2000. **168**(1-4): p. 108-113.
9. Carosella, C.A., et al., *Pulsed laser deposition of epitaxial BaFe[sub 12]O[sub 19] thin films*, in *Journal of Applied Physics*. 1992, AIP. p. 5107-5110.
10. Shinde, S.R., et al., *Effect of lattice mismatch strains on the structural and magnetic properties of barium ferrite films.* Applied Physics Letters, 1998. **72**(26): p. 3443-3445.
11. Shinde, S.R., et al., *Improvement in spin-wave resonance characteristics of epitaxial barium-ferrite thin films by using an aluminum-doped strontium-ferrite buffer layer.* Applied Physics Letters, 1999. **74**(4): p. 594-596.

12. Shinde, S.R., et al., *Realization of epitaxial barium ferrite films of high crystalline quality with small resonance losses.* Journal of Applied Physics, 1999. **85**(10): p. 7459-7466.
13. Song, Y.-Y., S. Kalarickal, and C.E. Patton, *Optimized pulsed laser deposited barium ferrite thin films with narrow ferromagnetic resonance linewidths.* Journal of Applied Physics, 2003. **94**(8): p. 5103-5110.
14. Oliver, S.A., et al., *Growth and characterization of thick oriented barium hexaferrite films on MgO (111) substrates.* Applied Physics Letters, 2000. **76**(24): p. 3612-3614.
15. Yoon, S.D. and C. Vittoria, *Microwave and magnetic properties of barium hexaferrite films having the c-axis in the film plane by liquid phase epitaxy technique.* Journal of Applied Physics, 2003. **93**(10): p. 8597-8599.
16. Kranov, Y.A., et al., *Barium Hexaferrite Thick Films Made by Liquid Phase Epitaxy Reflow Method.* Magnetics, IEEE Transactions on, 2006. **42**(10): p. 3338-3340.
17. Wang, S.G., S.D. Yoon, and C. Vittoria, *Microwave and magnetic properties of double-sided hexaferrite films on (111) magnesium oxide substrates.* Journal of Applied Physics, 2002. **92**(11): p. 6728-6732.
18. Lisfi, A., et al., *Barium Ferrite Films Grown by Laser Ablation.* IEEE Transactions on Magnetics, 1998. **34**: p. 1654-1656.
19. Hylton, T.L., M.A. Parker, and J.K. Howard, *Preparation and magnetic properties of epitaxial barium ferrite thin films on sapphire with in-plane, uniaxial anisotropy.* Applied Physics Letters, 1992. **61**(7): p. 867-869.
20. Yuan, M.S., H.L. Glass, and L.R. Adkins, *Epitaxial barium hexaferrite on sapphire by sputter deposition.* Applied Physics Letter, 1988. **53**.
21. Shockelford, J.F., *CRC Materials Science and Engineering Handbook*. 1992: CRC Press.
22. Wyckoff, R.W.G., *Crystal Structures*. 2nd ed. Vol. 2. 1964: John Wiley & Sons, Inc.
23. Dorsey, P.C., et al., *Coefficients of thermal expansion for barium hexaferrite.* Journal of Applied Physics, 1996. **79**(7): p. 3517-3520.

24. *Handbook of Crystal Growth*, ed. D.T.J. Hurle. Vol. 2. 1993: Elsevier Science.
25. Glass, H.L. and F.S. Stearns, *Growth of Hexagonal Ferrite Films by Liquid-Phase Epitaxy.* Ieee Transactions on Magnetics, 1977. **13**(5): p. 1241-1243.
26. Yoo, K.C., et al., *Investigation of growth conditions for the liquid phase epitaxy of hexaferrite films using a Bi2O3-BaO-B2O3 flux.* Journal of Crystal growth, 1987(85): p. 389-395.
27. Li, L., et al., *Substrate melting during thermal spray splat quenching.* Thin Solid Films, 2004(468): p. 113-119.